Research Square

Preprints are preliminary reports that have not undergone peer review.
They should not be considered conclusive, used to inform clinical practice,
or referenced by the media as validated information.

NAD+ depletion drives age-related monocyte hyperinflammation after stroke and is reversed by nicotinamide riboside

Mica Cabrera
The University of Texas at Austin
Hannah Ennerfelt
Stanford University School of Medicine
Abrar I. Alsaadi
Huck Institutes of the Life Sciences, Pennsylvania State University
Brent Eastman
Case Western Reserve University School of Medicine
Ludmila Alexandrova
Stanford University
Yeonglong Albert Ay
Stanford University School of Medicine
Jolie Huang
Stanford University
Qian Wang
Stanford University School of Medicine
Eran Blacher
The Hebrew University of Jerusalem
Melanie R. McReynolds
Huck Institutes of the Life Sciences, Pennsylvania State University
Katrin I. Andreasson
Stanford University School of Medicine
Chinyere Agbaegbu Iweka
cxi60@case.edu

Case Western Reserve University

Research Article

Keywords: Stroke, Aging, Inflammation, Metabolism, NAD+, Nicotinamide riboside, Quinolinic acid, Monocytes, Gut

Posted Date: September 12th, 2025

DOI: https://doi.org/10.21203/rs.3.rs-7483662/v1

License: This work is licensed under a Creative Commons Attribution 4.0 International License. Read Full License

Additional Declarations: No competing interests reported.

Version of Record: A version of this preprint was published at Journal of Neuroinflammation on November 27th, 2025. See the published version at https://doi.org/10.1186/s12974-025-03638-6.

Abstract

BACKGROUND: Aging exacerbates post-stroke inflammation, contributing to worse neurological outcomes. However, the mechanisms underlying this age-dependent immune dysregulation remain unclear. Because immune cell metabolism critically shapes inflammatory responses, we investigated whether the metabolic state of circulating monocytes, key immune cells that traffic to the ischemic brain, is altered by age after stroke. We further examined whether enhancing cellular NAD^+ availability with nicotinamide riboside (NR) could mitigate age-associated neuroinflammatory responses and improve stroke outcome.

METHODS: Ischemic stroke was induced in young and aged mice using the distal middle cerebral artery occlusion model. We assessed monocyte metabolic profiles via untargeted metabolomics, mitochondrial function assays, multi-analyte cytokine/chemokine profiling, and flow cytometry. Given the contribution of monocyte-derived intestinal macrophages to gut barrier disruption after stroke, we evaluated gut barrier integrity, immune cell composition, and systemic inflammation. Stroke outcomes were also determined by infarct size, motor function, and brain inflammatory status.

RESULTS: Our findings show that the availability of the essential energy co-factor, NAD^+, is a key age-dependent factor that regulates monocyte and intestinal macrophage immune responses after stroke. Aged monocytes showed decreased NAD^+ levels and increased inflammatory responses compared to young monocytes. Pretreatment with NR elevated cellular NAD^+ levels in aged monocytes, normalized intestinal macrophage numbers and activation states, preserved gut barrier integrity, reduced systemic and brain inflammation, and improved stroke outcomes in aged mice.

CONCLUSION: These findings highlight the importance of NAD^+ in mitigating the post-stroke response in aging and the potential of NAD^+ supplementation as a preventive strategy for patients at risk for cerebrovascular disease.

INTRODUCTION

An important consequence of acute ischemic stroke is secondary injury, which occurs as a result of robust and sustained immune cell infiltration into the ischemic brain, driven initially by monocytes and neutrophils.[1] This inflammatory response is significantly exacerbated in aged individuals compared to young.[2, 3] The underlying cause of this aggravated inflammatory response in aging remains unclear. Several studies have established that the metabolic state of immune cells plays a pivotal role in regulating immune responses, as metabolic reprogramming ensures sufficient energy for host defense and tissue homeostasis.[4] This metabolic homeostasis is disrupted with aging, impairing the ability to mount appropriate immune responses to stimuli.[5]

We hypothesized that energy metabolism could play a critical role in the immune responses to stroke in aged individuals. To study this, we investigated the metabolism of blood monocytes that along with neutrophils, are the first immune cells to infiltrate the ischemic brain where they differentiate into macrophages. In the ischemic area, macrophages clear cellular debris, promote repair, regeneration, and inflammation resolution; processes that depend on robust and adaptable energy metabolism.[4] The balance between glycolytic and oxidative metabolism can determine whether immune cells adopt an activated, pro-inflammatory state or maintain homeostatic regulatory functions.[6, 7] Homeostatic immune cells depend primarily on oxidative phosphorylation and fatty acid β-oxidation to generate ATP. However, upon activation, they shift toward aerobic glycolysis, also known as the Warburg effect.[7, 8] This metabolic shift fuels immune activation, with increased glucose utilization driving a pro-inflammatory phenotype in macrophages.[8] As glycolysis serves as a primary energy source for activated immune cells during inflammation, nicotinamide adenine dinucleotide (NAD^+), a key energy co-factor, is rapidly consumed to sustain this glycolytic activity and can potentially become limiting.[9] NAD^+ is critical for maintaining energy homeostasis and modulating immune function.[5] For example, inhibiting the *de novo* biosynthetic pathway for NAD^+ (downstream of the Kynurenine pathway) in aged, but not young macrophages, disrupts oxidative phosphorylation, impairs phagocytic function and the immune response to lipopolysaccharide (LPS).[5] NAD^+ levels decline significantly with age, impairing immune cell responses, while increasing cellular NAD^+ can enhance energy metabolism and reduce inflammation.[5, 10, 11]

In addition to trafficking to the ischemic brain, monocytes continually migrate to selected organs where they replenish macrophage populations, including the intestine, lung and spleen. Monocytes that traffic to the intestinal lamina propria function critically in maintaining intestinal homeostasis and gut barrier integrity.[12, 13] Following stroke, a burst of increased adrenergic input leads to transient opening of the gut barrier, translocation of microbial components, and hyper-activation of lamina propria macrophages, which in turn, further disrupts the gut epithelial barrier, leading to systemic bacterial dissemination.[14, 15]

In this study, we investigated the metabolic status of blood monocytes from young and aged mice at several time points after stroke. We also examined monocyte-derived lamina propria macrophages and the integrity of the gut barrier after stroke in young and aged mice. Our results

show that NAD^+ is critically dysregulated in blood monocytes from aged mice and is associated with disrupted immune responses and an accumulation of quinolinic acid (QA), a neurotoxic metabolite of the Kynurenine pathway. Prolonged pretreatment of aged mice with nicotinamide riboside (NR) to elevate cellular NAD^+ levels significantly improved monocyte energy metabolism, reduced inflammation, rescued the loss of lamina propria macrophages and gut barrier function after stroke. NR supplementation also significantly improved motor function and reduced infarct size following stroke.

MATERIALS AND METHODS

Animals

All experiments and procedures were performed in accordance with the National Institutes of Health (NIH) guidelines, and all protocols were approved by the Institutional Animal Care and Use Committee (IACUC) at Case Western Reserve University and Stanford University. All animals were socially housed in a pathogen-free barrier facility environmentally controlled for temperature and humidity, on a 12-hour light–dark cycle, with food and water available ad libitum. C57BL/6J mice were purchased from Jackson laboratories or obtained from the NIH aged rodent colony. Distal middle cerebral artery occlusion surgery and collection of all tissue samples were performed between *ZT2* and *ZT5* (*zeitgebers time*). This time interval was maintained to ensure consistency of any possible circadian effects and reduce variability.

Distal middle cerebral artery occlusion

Distal middle cerebral artery occlusion (dMCAo), a permanent coagulation of the middle cerebral artery via electrocoagulation was performed as described previously.[16] Young (3 – 6 months) and aged (18 – 20 months) C57BL/6J male mice were anesthetized with 3% isoflurane and then with 70% N_2O + 30% O_2 maintained throughout the surgical procedure, and injected intramuscularly with 0.3 mg/kg buprenorphine (BERLAB0.5-232305; ZooPharm, Laramie, WY). The mice were placed on a heating blanket at 37˚C to maintain body temperature. Eye ointment (Artificial Tears Ophthalmic Lubricant, Akorn, Inc. Lake Forest, IL) was applied to both eyes to prevent dryness during the procedure. The mice were randomized and subjected to either dMCAo or sham surgery which involved thinning of the skull without coagulation of the middle cerebral artery.

Nicotinamide Riboside (NR) treatment

Mice were administered with either water (vehicle) or 400 mg/kg of nicotinamide riboside (NR; ASB-000114315-101; Niagen; Chromadex, Irvine CA) daily via oral gavage at the same time of day (between *ZT*2–3) for 4 weeks. Mice were weighed and values recorded every week and no adverse reactions to NR was observed. Certificates of Analysis provided by the manufacturer and performed on separate lots reported ~ 99% purity of the NR preparation.

Immunofluorescence

Mice were euthanized in CO_2 chamber and transcardially perfused with 10 mM PBS. Brain and gut tissue were isolated and immersed in 4% paraformaldehyde (PFA; 15714-1L; Electron Microscopy Sciences, Hatfield, PA) overnight and then serially cryopreserved in 15% sucrose and then 30% sucrose solution. 1 cm gut tissue sections were collected from the duodenum, jejunum and ileum and embedded in optimal cutting temperature compound (O.C.T, 23-730-571; Fisher Scientific, Waltham, MA) and then longitudinally sectioned at 10 µm per section. Four sections per mouse were mounted on Superfrost Plus slides (Thermo Fisher Scientific, Waltham, MA) and immunostained. For each brain, five 40 µm brain sections were coronally sectioned using a sliding microtome (Microm HM430, Thermo Fisher Scientific, Waltham, MA) at 500 µm intervals between approximately 1.5 mm rostral and 1.5 mm caudal to bregma. Brain tissue slices were placed in freezing media and stored at – 20˚C. Briefly, both brain and gut tissue samples were washed 3× in PBS for 5 minutes and permeabilized in 0.2% Triton-X100 in PBS for 20 minutes at room temperature. Samples were then washed in 10 mM PBS and incubated for 1 hour in blocking buffer (0.2% Triton-X100 supplemented with 10% normal donkey serum in 10 mM PBS) and then in primary antibody (see appendix for list of antibodies) overnight at 4˚C. Next, the samples were washed 3× in PBS for 5 minutes and then incubated in secondary antibody (see appendix for the list of antibodies) for 2 hours. Samples were washed 3× in 10 mM PBS for 5 minutes and then incubated in Hoechst stain for 10 minutes in 10 mM PBS. Samples were washed in 10 mM PBS and then mounted with Prolong™ Gold antifade reagent (P36930; Invitrogen, Eugene, OR), and tissue samples mounted onto Superfrost Plus slides (Thermo Fisher Scientific, Waltham, MA). Gut tissue sections were acquired on Zeiss 780 LSM confocal microscope (Carl Zeiss, Thornwood, NY) using either 20×/0.45 NA dry objective lens or 40×/0.95 NA oil immersion objective lens. Mean fluorescence intensity was quantified using ImageJ (http://imagej.nih.gov/ij).

Quantification of stroke infarct area

Measurement of infarct area was carried out by an investigator blinded to treatment. 40 µm brain slices were immunostained with MAP2 to delineate infarcted area which had a relatively high fluorescent signal due to dead and dying neurons, and IBA1 and CD68 to quantify microglia (see appendix for antibody details). Images were acquired using a 10× objective lens with a 0.40 NA on a Leica SP8 confocal microscope (Leica Microsystems Inc, Deerfield, IL). Infarct area was quantified using ImageJ (http://imagej.nih.gov/ij).

Blood monocyte isolation

Blood was collected by transcardiac puncture from mice with 0.25 mM EDTA (anticoagulant) and mixed with ACK lysing buffer (A1049201; Thermo Fisher Scientific, Waltham, MA). Samples were incubated on ice for 15 minutes and centrifuged at 300 ×g for 6 minutes. Samples were then resuspended in 10 mM PBS containing 2% FBS and 1 mM EDTA. EasySep™ mouse monocyte isolation kit (19861; STEMCELL Technologies, Vancouver, BC, Canada) was used to isolate and enrich blood monocytes by immunomagnetic negative selection.

Chemokine and cytokine multiplex assay – Luminex

Briefly, blood was collected by transcardiac puncture from mice with 0.25 mM EDTA, and either centrifuged at 2000 ×g at 4˚C for 10 minutes and blood plasma collected, or blood monocytes isolated using the EasySep™ mouse monocyte isolation kit (19861; STEMCELL Technologies, Vancouver, BC, Canada). Mice were perfused with 10 mM PBS and brain tissue was collected from each mouse. Cells and tissue samples were lysed with cell lysis buffer (RIPA buffer; 89901; Thermo Fisher Scientific, Waltham, MA) and protein quantified by BCA (A55864, Thermo Fisher Scientific, Waltham, MA). Equal concentrations of samples were stored at – 80°C and cytokine analysis was carried out at the Human Immune Monitoring Core (Stanford University, CA) using magnetic bead-based multiplex Luminex assays (LXSAMSM; R&D Systems, Inc., Minneapolis, MN). Plates were read using a Luminex LabMap200 instrument. Mean fluorescence intensity (MFI) was averaged over duplicate wells for each cytokine per sample on each plate.

Endotoxin Lipopolysaccharide Assay

Briefly, blood was collected by transcardiac puncture from mice with 0.25 mM EDTA. Samples were centrifuged at room temperature for 10 minutes at 2500 rpm. Blood plasma was removed and tested for bacterial lipopolysaccharide (LPS) using the LPS ELISA kit (MBS261904; Mouse Lipopolysaccharide ELISA Kit; MyBioSource, Inc. San Diego, CA).

FITC-Dextran

Mice were fasted for 4 hours with *ad libitum* access to water at the beginning of the light cycle at *ZT*0, 24 hours post stroke. Blood samples were collected via tail snip, centrifuged at 5000 rpm for 10 minutes at room temperature and kept on ice. Then 80 mg/mL of 4 kDa FITC-dextran (46944-500MG-F; Millipore Sigma, St. Louis, MO) diluted in sterile 10 mM PBS (per mouse) was administered via oral gavage. 4 hours post-administration, blood samples were collected via transcardiac puncture with 0.25 mM EDTA, centrifuged at 5000 rpm at room temperature for 10 minutes. Blood plasma was removed and the levels of FITC-dextran measured with a fluorescent plate reader.

Real-Time Oxygen Consumption Rate (OCR) and Extracellular Acidification Rate (ECAR)

Blood monocytes were isolated using the EasySep™ mouse monocyte isolation kit (19861; STEMCELL Technologies, Vancouver, BC, Canada) from each mouse as described previously and seeded in a seahorse XFe24 cell culture microplate (102340-100; Agilent, Santa Clara, CA) and allowed to adhere for 1 hour at 5% CO_2 at 37°C. Cells were washed twice with Agilent seahorse XF Media (103680-100; Agilent, Santa Clara, CA) supplemented with 1 mM pyruvate (Gibco™ 11360070; Fisher Scientific, Waltham, MA), 2 mM L-glutamine (400-106-100; GeminiBio, West Sacramento, CA) and 2 mM D-glucose (G7021-1KG; Sigma-Aldrich, St. Louis, MO) in a final volume of 500 µL. Cells were then incubated in a 0% CO_2 chamber at 37°C for 1 hour before being placed into a seahorse XFe24 analyzer (US421134; Agilent, Santa Clara, CA). Cells were treated with 2.5 µM oligomycin, 2 µM carbonyl cyanide p-trifluoromethoxyphenylhydrazone (FCCP), and 0.5 µM rotenone/antimycin (103015-100; Seahorse XF Cell Mito Stress Test Kit; Agilent, Santa Clara, CA). 1 µM of Hoescht (H3570; Invitrogen, Waltham, MA) was injected at the end of the assay for cell counting. A total of three OCR and pH measurements were taken after each compound was administered from which basal respiration, maximal respiration, ATP production, spare respiratory capacity and extracellular acidification rates were calculated. All values were normalized by Hoescht-positive cell counting in the Cytation1 imaging platform (20081913; Agilent, Santa Clara, CA).

Flow cytometry sample preparation

The small intestine (SI) was removed following perfusion and placed in cold 10 mM PBS. The SI was then cut into segments that underwent cleaning by flushing with cold sterile 10 mM PBS. Gut segments were then cut open and into 2 cm pieces before being placed in dissociation

buffer: HBSS (without calcium/magnesium) containing 1% 0.5M EDTA and 1% HEPES and placed on a shaker at 180 rpm at 37˚C for 40 minutes. Following incubation, samples were poured through a 70 µm strainer and the flow-through was discarded. The tissue on the strainer was then moved to a new tube and dissociated mechanically with scissors for ~ 30 seconds. Samples were resuspended in HBSS (without calcium/magnesium) containing 2% FBS, 0.5 mg/mL collagenase E and 0.5 mg/mL DNase I and placed on the shaker at 180 rpm at 37˚C for 45 minutes. Samples were again filtered through a 70 µm strainer and washed with 10 mL of cold HBSS (without calcium/magnesium). Samples were then centrifuged at 1400 rpm for 8 minutes at 4˚C and the supernatant discarded. Samples were washed again with 5 mL of HBSS (without calcium/magnesium) and centrifuged at 1400 rpm for 8 minutes at 4˚C. Supernatants were discarded and cell pellets resuspended in FACS buffer before staining for flow cytometry.

Flow cytometry procedure

Samples were transferred to a 96-well v bottom plate (277143; Thermo Fisher Scientific, Waltham, MA), and washed 1× with FACS buffer (500 mL of 10 mM PBS containing 1 mL of 0.5M EDTA, and 1 g of Bovine Serum Albumin; BSA). Gut cells were stained at a dilution of 1:200 with CD11b (BV421), Ly6G (BV605), Ly6C (V450), CD45 (AF 700), MHCII (PerCP-efluor710), EGR2 (PE-Cy7), Live Dead Aqua, and with 1:1000 FC block in in FACS buffer for 25 minutes at 4°C. The cell pellets were centrifuged at 500 ×g for 3 minutes and then washed with FACS buffer then resuspended in 200 µL of FACS buffer and run on Cytek Aurora flow cytometry instrument (Fremont, CA). Analysis was performed using FlowJo software v10.

Metabolomics

Water Soluble Metabolites: A solvent mixture of 80:20 methanol/water (500 µL) containing seven internal standards was used to resuspend the pellets that were composed of blood monocytes isolated from mice. Cell suspensions were vortexed for 30 seconds, sonicated in a water bath (30 seconds sonication, 30 seconds on ice, repeated 3 times), vortexed for 30 seconds and incubated for 2 hours at − 20°C to allow for protein precipitation. The supernatant was collected after centrifugation at 10,000 rpm for 10 minutes at 4°C and then evaporated to dryness under nitrogen. The dry extracts were then reconstituted with 100 µL of 50:50 methanol/water before analysis. Supernatants were centrifuged at 16,000 ×g for 20 minutes to remove any residual debris before analysis. Extracts were analyzed within 36 hours by liquid chromatography coupled to a mass spectrometer (LC − MS). The LC–MS method involved hydrophilic interaction chromatography (HILIC) coupled to the Q Exactive PLUS mass spectrometer (Thermo Fisher Scientific, Waltham, MA) as previously described.[17] The LC separation was performed on a XBridge BEH Amide column (150 mm 3 2.1 mm, 2.5 mm particle size; Waters, Milford, MA). Solvent A was 95%:5% H_2O: acetonitrile with 20 mM ammonium bicarbonate, and solvent B was acetonitrile. The gradient was 0 min, 85% B; 2 min, 85% B; 3 min, 80% B; 5 min, 80% B; 6 min, 75% B; 7 min, 75% B; 8 min, 70% B; 9 min, 70% B; 10 min, 50% B; 12 min, 50% B; 13 min, 25% B; 16 min, 25% B; 18 min, 0% B; 23 min, 0% B; 24 min, 85% B; 30 min, 85% B. Other LC parameters were: flow rate, 150 mL/min; column temperature, 25˚C; injection volume, 10 µL; and autosampler temperature, 5˚C. The mass spectrometer was operated in both negative and positive ion mode for the detection of metabolites. Other MS parameters were: resolution of 140,000 at m/z 200, automatic gain control (AGC) target at 3^6, maximum injection time of 30 ms and scan range of m/z 75-1000. Raw LC/MS data were converted to mzXML format using the command line “msconvert” utility.[18] Data was processed and analyzed using MAVEN software (Princeton University, Princeton, NJ). Significant metabolites were formally identified by matching fragmentation spectra to public spectral libraries or by matching retention time and fragmentation spectra to authentic standards when possible.

Determination of the NAD^+, Kynurenine pathway and related metabolites

Analyte standards for NAD^+ metabolites

The following standards (see appendix for list of reagents catalogue numbers) Nicotinamide (NAM); Nicotinamide mononucleotide (NMN); nicotinamide adenine dinucleotide (NAD^+); nicotinic acid mononucleotide (NaMN); nicotinic acid adenine dinucleotide (NaAD); adenosine monophosphate (AMP); adenosine diphosphate ribose (ADPr); NAM-d4; $AMP^{15}N_5$ were purchased from either Medical Isotopes, Inc, or Sigma-Aldrich (St. Louis, MO). For NaMN-d4 standard, the M + 4 D/molecule was significantly less than the M + 3 isotopomer and significantly less than the unlabeled molecular ion peak at identical concentrations in solution. Therefore, the actual incorporation of deuterium in NaMN-d4 was determined by mass spectrometry analysis where M + 3 D/molecule was the major isotopomer and NaMN-d3 was used as an internal standard for the quantification.

Analyte standards for the Kynurenine pathway metabolites

The following standards (see appendix for list of reagents catalogue numbers) L-Tryptophan (TRP); Kynurenine (KYN); 3 Hydroxy DL-Kynurenine (3HK); Kynurenic acid (KA); 3 Hydroxyanthranilic acid (3HANA); Quinolinic acid (QA); TRP-d5; and KA-d5 – were purchased from Sigma-Aldrich (St. Louis, MO). KYN-d4; 3HK-d3; 3HANA-d3 and QA-d3 were purchased from Medical Isotopes, Inc.

Calibration curve preparation

Individual analytes and internal standard (IS) primary stock solutions include: 10 mM (NAM; NMN; NaMN, NaAD; ADPr): 20 mM (NAD+; AMP); 2 mM (NAD^+-d4); 5 mM (NaMN-d3) and 10 mM (NAM-d4; NMN-d4; AMP-15N5), were prepared individually in water corrected for lot purity and salt. For the Kynurenine pathway metabolites, individual analytes and corresponding internal standards (IS) 10 mM primary stock solutions were prepared separately in water containing 0.1% formic acid and 0.02% ascorbic acid corrected for lot purity. Intermediate stock solutions were prepared by mixing individual stock solutions of each analyte followed by dilution. These intermediate stock solutions were serially diluted with water to obtain a series of standard spiking solutions, which were used to generate the calibration curve. Calibration curves were prepared by spiking 10 µL of each standard working solution into 25 µL of homogenization buffer (0.5N perchloric acid in water) followed by addition of 10 µL internal standard solutions. For NAD^+ metabolites: 4 µM for NAD^+-d4 and AMP-15N5; 2 µM for NAM-d4; NMN-d4 and NaMN-d3. A calibration curve was prepared fresh with each set of samples. Using 25 µL aliquots, the calibration curve range for NAD^+ and AMP was 0.016–160 µM; for NAM; NMN; NaMN; NaAD; and ADPr was 0.008–80 µM.

Calibration curves for the Kynurenine pathway metabolites were prepared likewise. Final concentration of IS in the sample was 4000nM for TRP-d5; 400nM for QA-d3, 3HANA-d3, 3HK-d3 and 200nM for KYN-d4 and KA-d5. A calibration curve was prepared fresh with each set of samples. Using 25 µL aliquot the calibration curve range for TRP 4 nM – 20 uM; KYN 0.4–4000 nM; KA 0.4–1000 nM; 3HK 2–4000 nM; 3HANA and QA 10–4000 nM.

Sample collection and extraction procedure

The extraction procedure was modified from that of Liang X. et al.[19] Samples isolated from mice include blood monocytes, infarcted cortex, and gut. Samples were weighed and placed into lysing matrix D vials containing 1.4 mm zirconium-silicate spheres (1169130-CF; MP Biomedicals, Solon, OH); snap-frozen with liquid nitrogen and kept frozen at -80°C until analysis. Before LC-MS/MS analysis, samples were removed from the − 80°C freezer and placed on ice. A cold solution of 0.5N perchloric acid was added to frozen samples in the following amounts: Monocytes – 100 µL; cortex and gut – 200 µL. Samples were homogenized using Bead Mill-4 (15-340-164; Thermo Fisher Scientific, Waltham, MA) twice at 30 seconds at a speed of 5 m/s and then centrifuged. 25 µL of supernatant was used for analysis. 10 µL internal standard solution and 10 µL water solution was added to 25 µL aliquots of supernatant and vortexed. For the NAD^+ metabolites, samples were diluted with 60 µL 20mM ammonium formate buffer with 0.1% formic acid in water, vortexed, centrifuged, transferred to injection vial and analyzed by LC-MS/MS. For the Kynurenine pathway metabolites, samples were diluted with 40 µL 20mM ammonium formate buffer with 0.1% formic acid in water, vortexed, centrifuged, transferred to injection vial and analyzed by LC-MS/MS.

LC-MS/MS

Since some of the analytes namely NMN/NaMN and NAD^+/NaAD have a mass difference of 1 amu, chromatographic separation is critical. At least two selective reaction monitoring (SRM) transitions – one quantifier and one qualifier – were carefully selected for each analyte. Distinctive qualifier to quantifier ion intensity ratios and retention times were essential to authenticate the target analytes. All analyses were carried out by positive electrospray LC-MS/MS using a Waters Acquity I-class LC system with Waters Xevo TQ-XS triple quadrupole mass spectrometer (RRID:SCR_018510). Chromatographic conditions include: Atlantis® T3, 2.1x100 mm, 3 µm particle size column (186003718; Waters Corp. Milford, MA) was operated at 30°C with a flow rate of 0.2 mL/min. Mobile phases consisted of A: 20 mM ammonium formate/0.1% formic acid in water and B: 20 mM ammonium formate/0.1% formic acid in acetonitrile/methanol/water (45:45:10). Elution profile include: initial hold at 0% B for 3 minutes, followed by a gradient of 0%-30% in 6 minutes, then 30%-95% in 2 minutes, hold at 95% for 1 minute; total run time was 15 minutes. Injection volume was 10 µL.

SRM was used for quantification. The mass transitions were as follows: NAM: m/z 122.58 → m/z 105.42 (quantifier); m/z 122.58 → m/z 79.35 (qualifier); NMN: m/z 335.03 → m/z 122.49 (quantifier); m/z 335.03 → m/z 96.37 (qualifier); NaMN: m/z 336.03 → m/z 123.46 (quantifier); m/z 336.03 → m/z 96.36 (qualifier); ADPr: m/z 560.03 → m/z 135.59 (quantifier) and m/z 560.03 → m/z 347.96 (qualifier); NAD^+: m/z 664.16 → m/z 135.55 (quantifier) and m/z 664.16 → m/z 428.09 (qualifier); NaAD: m/z 665.16 → m/z 135.56(quantifier) and m/z 665.16 → m/z 428.04 (qualifier); AMP: m/z 347.93 → m/z 135.56 (quantifier) and m/z 347.93 → m/z 118.49 (qualifier); NAM-d4: m/z 126.58 → m/z 83.16 ; NMN-d4: m/z 339.03 → m/z 126.53; NaMN-d3: m/z 338.5 → m/z 126.54; NAD^+-d4: m/z 668.16 → m/z 135.56; and AMP 15N5: m/z 353.19 → m/z 140.60. Dwell time was 25 ms.

For the Kynurenine pathway metabolites, the mass transitions were as follows: TRP: m/z 204.776 → m/z 131.594 (quantifier); m/z 204.776 → m/z 117.525 (qualifier); KYN: m/z 208.72 → m/z 93.427 (quantifier); m/z 208.72 → m/z 117.516 (qualifier); 3HK: m/z 224.776 → m/z 109.528 (quantifier); m/z 224.776 → m/z 165.654 (qualifier); KA: m/z 189.656 → m/z 143.548 (quantifier) and m/z 189.656 → m/z 115.546 (qualifier); 3HANA: m/z 153.584 → m/z 107.504 (quantifier) and m/z 153.584 → m/z 135.576 (qualifier); QA: m/z 167.584 → m/z 105.479 (quantifier) and m/z 167.584 → m/z 77.314 (qualifier); TRP-d5: m/z 209.84 → m/z 149.711 ; KYN-d4: m/z 212.84 → m/z 97.492; 3HK-d3: m/z 227.784 → m/z 110.708; KA-d5: m/z 194.72 → m/z 93.245; and 3HANA-d3: m/z 156.648 → m/z 138.591; QA-d3 m/z 170.648 → m/z 108.497. Dwell time was also 25 ms.

Quantification

Quantitative analysis was done with TargetLynx quantification software (Waters Corp. Milford, MA) using an internal standard approach. NAM-d4; NMN-d4; NaMN-d3 were the internal standards used for quantification of NAM; NMN; NaMN, respectively; NAD^+-d4 for NAD^+ and NaAD; and AMP15N5 for AMP and ADPr. TRP-d5; KYN-d4; 3HK-d3; KA-d5; 3HANA-d3 and QA-d3 were the internal standards for quantification of TRP; KYN; 3HK; KA; 3HANA and QA, respectively. Calibration curves were linear ($R > 0.98$) over the concentration range using a weighting factor of 1/X2 where X is the concentration. The back-calculated standard concentrations were ± 15% from nominal values, and ± 20% at the lower limit of quantitation (LLOQ).

Rotarod

The rotarod test was used to evaluate motor function and coordination. Mice were pretrained on the rotarod for one week before stroke was induced, with 3 trials separated by 15-minute inter-trial intervals. The mice were kept on the rotarod until they learned to stay on for 300 sec. Training began with a constant low-speed rotation (5 rpm) for 5 minutes on the first day of training. On all subsequent days, each mouse was placed on the rod with the rotation speed increasing from 4–40 rpm (ramping) over 5 minutes. Testing was performed on the day before stroke and the day after stroke and involved placing the mice on the rotarod for a maximum of 300 sec and measuring the length of time they remained on the rotarod with ramping, and reverse ramping speeds before falling on the soft pad below. The rotarod (Ugo Basile, Italy) consisted of a striated rod (consisting of 5 lanes with diameter: 3 cm; rod width: 5.8 cm; fall height: 16 cm).

Statistical analysis

For all experiments, mice were randomly assigned to either sham, stroke, vehicle-treated or NR-treated groups. Investigators were blinded to group allocation during data collection and analysis. No power analysis was performed to determine sample sizes; prior literature using similar experimental paradigms that yielded interpretable results and the laboratory's previous experience was used.[14] All analyses were performed using either GraphPad Prism software version 10 (GraphPad Software, LaJolla, CA), R statistical package software version R 4.4.0, or Metaboanalyst 6.0. Unless otherwise specified, values represent the means ± SEM of at least three independent experiments. Data were analyzed by unpaired Student's *t*-test with Welch's correction, one-way ANOVA, two-way ANOVA or repeated measures two-way ANOVA with Tukey's posthoc or Bonferroni multiple comparison test to determine significance. Normality of the distribution of the data was tested with Kolmogorov–Smirnov normality tests using the column statistics function of GraphPad Software. Metabolomics data analysis was carried out using MetaboAnalyst 6.0. Metabolomic data were log-transformed and scaled according to the auto-scaling feature (mean-centered and divided by the standard deviation of each variable). Metabolites that were significantly different by ANOVA (with FDR correction) were subjected to hierarchical clustering analysis using the Euclidean distance measure and Ward clustering algorithm. Differentially expressed metabolites underwent pathway-based enrichment analysis using 84 metabolite sets based on KEGG metabolic pathways in MetaboAnalyst 6.0.

RESULTS

Aging impairs blood monocyte energy metabolism after stroke.

To evaluate acute age-dependent changes in the energy metabolism of blood monocytes in response to stroke, we subjected young (3–6 month) and aged (18–20 month) male mice to distal middle cerebral artery occlusion (dMCAo), and isolated blood monocytes at 4.5 hours, 24 hours and 72 hours post stroke (Fig. 1A). We assessed the metabolic function of blood monocytes using a Mitostress test that induces mitochondrial stress to measure basal respiration (BR) and ATP production, indicators of oxidative phosphorylation, and extracellular acidification rates (ECAR), an indicator of glycolytic activity. At 4.5 hours after stroke, there were no differences in BR, ATP production or ECAR in the blood monocytes from young stroke compared to sham mice (Fig. 1B and 1C). Significant increases in BR and ATP production but no changes in ECAR were observed in aged stroked compared to sham mice (Fig. 1B and 1C). At 24 hours post stroke, BR was moderately reduced and ATP production and ECAR were significantly lower in young stroked mice compared to sham (Fig. 1B and 1C). In aged stroked mice, while previously increased at 4.5 hours, BR, ATP production and ECAR were significantly reduced (Fig. 1B and 1C), suggesting metabolic exhaustion in the blood monocytes compared to aged sham. By 72 hours after stroke, all metabolic parameters rebounded to sham levels in young mice, while in aged stroked mice, the decrease in BR and ATP production persisted with ECAR unchanged, suggesting that the blood monocytes remained metabolically depleted (Fig. 1B and 1C).

Together, these results indicate that blood monocytes in young stroked mice experience a brief depletion of metabolic reserves under stress at 24 hours post stroke, followed by recovery. In contrast, blood monocytes in aged stroked mice initially exhibit an elevated metabolic response, engaging both oxidative phosphorylation and glycolysis to fuel their activation followed by a prolonged phase of metabolic exhaustion.

Age-dependent changes in blood monocyte NAD^+ and quinolinic acid levels following stroke.

To further explore the metabolic response of blood monocytes following stroke, we conducted metabolomic analyses to identify stroke-induced alterations in metabolic pathways and assess how these changes are affected by age (Figure S1–S3). Enrichment pathway analyses revealed changes in the nicotinamide adenine dinucleotide (NAD^+) metabolic pathway at all time-points in aged stroked mice that were absent in young mice (Fig. 1D and Figure S4A–C). NAD^+ plays a critical role in specifying immune responses in aged mice,[5, 20] and is synthesized via three major pathways: the Preiss-Handler, Salvage and the Kynurenine pathways (KP), also known as the NAD^+ *de novo* biosynthetic pathway.[21] The KP is a significant source of NAD^+ during an immune challenge,[5] and has been shown to be activated in stroke patients.[22, 23] Activation of the KP has been linked to stroke severity, with higher kynurenine/tryptophan ratios observed in the blood plasma of patients who died from stroke.[22] Quinolinic acid (QA), a metabolite of the KP, which is converted to the NAD^+ precursor nicotinamide adenine mononucleotide (NaMN), is a neurotoxic molecule that binds *N*-methyl-*D*-aspartate (NMDA) receptors to induce excitotoxicity in neurons, and is a potent mediator of inflammation.[24, 25]

Therefore, we investigated if stroke regulates NAD^+ and QA levels in blood monocytes in an age-dependent manner. At 4.5 hours after stroke, we found no differences in NAD^+ levels in the blood monocytes from young mice (Fig. 1E), however, NAD^+ was significantly increased in blood monocytes from aged stroked mice compared to sham (Fig. 1F). At 24 hours post-stroke, NAD^+ levels in blood monocytes from young mice were significantly elevated (Fig. 1E). In contrast, while aged mice exhibited increased NAD^+ at 4.5 hours post-stroke, levels were significantly reduced by 24 hours, indicating NAD^+ depletion (Fig. 1F). At 72 hours post stroke, NAD^+ levels of blood monocytes from young and aged stroked mice had rebounded to sham levels (Fig. 1E and 1F).

QA levels were increased in blood monocytes from young and aged mice at 4.5 hours post stroke (Fig. 1E and 1F). The increase in QA persisted at 24 hours post stroke in both young and aged mice (Fig. 1E and 1F). However, by 72 hours post stroke, QA levels rebounded to sham levels in young mice but remained elevated in aged stroked mice (Fig. 1E and 1F). Overall, these results suggest that the Kynurenine pathway (KP) is activated to boost NAD^+ production in blood monocytes after stroke in both young and aged mice. However, in aged mice, the conversion of quinolinic acid (QA) to the NAD^+ precursor NaMN appears to be impaired, resulting in QA accumulation (Figure S4D).

Replenishing NAD^+ levels increases oxygen consumption rates in blood monocytes from aged mice after stroke.

Nicotinamide riboside (NR) increases NAD^+ levels, improves metabolism, reduces inflammation in human monocyte-derived macrophages, and attenuates neuronal loss in a mouse model of acute ischemia.[10, 11, 26–28] These findings are based on studies in young mouse models and not aged mice, which are more representative of human stroke populations. Here, we tested whether NAD^+ regulates blood monocyte function during stroke in an age-dependent manner. Therefore, we administered either vehicle (water) or NR to young and aged mice via oral gavage every day for 4 weeks and then subjected the mice to stroke (Figure S5A). Blood monocytes were isolated at 24 hours post stroke, given that we observed the most distinct age-related metabolic differences at this time-point. A Mitostress test revealed no differences in basal respiration (BR) and ATP production between vehicle and NR-treated young stroked mice, however, there was a significant decrease in ECAR, suggesting reduced glycolytic rates (Fig. 2A). In aged stroked mice, BR, ATP production and ECAR were all significantly increased with NR treatment (Fig. 2A), consistent with improved oxidative phosphorylation and glycolysis.

To determine if NR increased NAD^+ levels via the KP, we measured NaMN as a readout for increased flux through the Priess-Handler and KP, as demonstrated in previous studies.[26, 29] This approach was chosen given the limitations of directly measuring NAD^+ in small sample sets such as blood monocytes. In the blood monocytes from young mice, there were no differences in NaMN levels between vehicle and NR-treated stroked mice (Fig. 2B). However, in the aged stroked mice, NaMN levels were significantly increased (Fig. 2B), suggesting NR may have improved QA conversion to NaMN. To confirm that QA was converted to NaMN, we measured QA levels. Indeed, NR modestly decreased QA levels in blood monocytes from young stroked mice, and significantly reduced QA levels in aged stroked mice compared to vehicle-treated mice (Fig. 2B). Together, these results suggest that prolonged pretreatment with NR decreased the stroke-induced increase in QA levels in blood monocytes from aged mice.

Nicotinamide riboside reduces the inflammatory response of blood monocytes after stroke in aged mice.

To determine if the inflammatory response of blood monocytes correlates with changes in their metabolic state, we measured immune factors in isolated blood monocytes using a chemokine and cytokine multiplex assay. At 4.5 hours post stroke, macrophage chemoattractant protein/C-C ligand 7 (MCP3/CCL7), a chemokine that plays a role in monocyte/macrophage/neutrophil recruitment through activation of the janus kinase/signal transducer and activator of transcription (JAK/STAT) pathway to induce cell proliferation and survival,[30] was the only immune factor increased in the blood monocytes from young stroked mice compared to sham including IL-7Rα (Fig. 2C). In aged stroked mice, several immune factors were increased, including MCP3/CCL7, indicating increased monocyte cell proliferation, monocyte

differentiation, and migration. At 24 hours post stroke, in blood monocytes from young stroked mice, we detected a decrease in macrophage colony-stimulating factor (MCSF1), a cytokine required for monocytic differentiation into macrophages.[31] However, in aged stroked mice, there was an increase in the expression of several immune factors that play roles in monocytic activation, proliferation, migration and differentiation (Fig. 2C). By 72 hours post stroke, we detected no differences in young mice, while the increase in IL-7Rα persisted in aged stroked mice (Fig. 2C). IL-7Rα expression promotes antimicrobial activity in monocytes,[32] indicating a potential response to elevated bacterial load resulting from increased gut barrier permeability after stroke.[15, 33]

Next, we measured immune factors in the blood plasma as indicators of systemic, whole-body inflammation. We observed changes in inflammation over time and age-related differences that were exacerbated by stroke (Figure S5B–D). A majority of these immune factors converge on the JAK/STAT pathway to mediate immune cell proliferation, activation, differentiation and migration as well as downstream signaling to promote inflammation. While young mice exhibited only a mild systemic inflammatory response to stroke within 72 hours, aged mice showed an initially modest response that intensified by 24 hours post stroke before subsiding by 72 hours (Figure S5B–D).

Next, to determine whether NAD^+ replenishment from pretreatment with NR could influence stroke-induced inflammation, we measured immune factors in blood monocytes from vehicle and NR-treated young and aged mice 24 hours after stroke. No significant differences in any immune factors were observed due to NR treatment in young stroked mice (Fig. 2D). However, NR reduced levels of several inflammatory factors that were increased in the blood monocytes from aged stroked mice (Fig. 2E). We also investigated the effect of NR on systemic inflammation by measuring the levels of immune factors in the blood plasma from sham, vehicle and NR-treated young and aged stroked mice. We observed no differences between all groups of young mice (Figure S6B), however there was a significant reduction in stroke-induced inflammation in aged stroked mice following NR treatment (Figure S6C).

Altogether, these results show a marginal effect of NR on blood monocyte and systemic inflammation in young mice, while in aged mice, NR has significant suppressive effect on stroke-mediated inflammatory responses.

Nicotinamide riboside alters stroke-induced inflammation in the ipsilateral and contralateral cortex.

Next, we tested whether NR might also regulate inflammation in the brain of stroked mice. We isolated the ipsilateral infarct core and a corresponding area in the contralateral brain at 24 hours post stroke in vehicle and NR-treated young and aged stroked mice and performed a chemokine and cytokine multiplex assay. We determined that NR reduced all detected immune factors in the ipsilateral cortex of both young and aged stroked mice, with the exception of IL-1α and MDC/CCL22 in the aged stroked mice (Fig. 3A), both of which were increased and play a role in immune cell recruitment and regulation. In the contralateral cortex of young stroked mice, we observed no effect of NR on the expression of immune factors (Fig. 3B). In aged mice, however, several cytokines and chemokines were decreased while others were elevated, indicating an altered inflammatory response in the contralateral cortex (Fig. 3B).

We then assessed the effect of NR pretreatment on brain NAD^+ levels. NR increased NAD^+ levels in the contralateral cortex of young mice but did not affect NAD^+ levels in the ipsilateral cortex, while in aged stroked mice, NR significantly elevated NAD^+ levels in both hemispheres (Fig. 3C and 3D). These results suggest that NR alters the immune response in both the ipsilateral and contralateral hemispheres in aged mice following stroke, and these changes may be due to the levels of NAD^+ availability in the brain.

Nicotinamide riboside changes the composition of macrophage cell populations in the gut.

Monocytes traffic to the gut lamina propria where they critically maintain the gut barrier,[12] which becomes compromised following stroke.[15, 33] Therefore, we investigated effects of NR pretreatment on lamina propria macrophage cell composition using flow cytometry (Figure S6A). The number of gut monocyte-derived macrophages (MDMs) identified as $CD45^+$ $CD11b^+$, $Ly6C^+$, $F4/80^+$ cells (Figure S6A) and tissue resident macrophages (TRMs), identified as $CD45^+$ $CD11b^+$, $Ly6C^+$, $CD62L^+$ cells (Figure S6A) did not change with stroke at 24 hours but was significantly increased with NR treatment in young mice (Fig. 4A). In aged mice, stroke significantly reduced the populations of gut MDMs and TRMs, however this was completely prevented by NR pretreatment (Fig. 4A), suggesting a beneficial effect of increased cellular NAD^+ in gut macrophages and/or broadly across the gut epithelium.

Next, we investigated the populations of P1 (newly infiltrating inflammatory monocytes – $Ly6C^{Hi}$ $MHCII^{Low}$), P2 (inflammatory monocytes – $Ly6C^{Int}$ $MHCII^{Hi}$) and P3 (new tissue resident macrophages – $Ly6C^{low}$ $MHCII^{Hi}$) cells in the gut that consists of both MDMs and TRMs.[34] The populations of P1, P2 and P3 macrophages were decreased with stroke in aged but not young stroked mice, and NR prevented loss of the P1 populations in aged stroked mice (Fig. 4B). To further characterize the polarization states of gut macrophages, we assessed the number of cells positive for CD71 (marker for proliferating macrophages and required for phagocytosis),[35] and MHCII (marker for activated macrophages and antigen presentation).[36] In the gut of both young and aged stroked mice, NR increased the populations of $CD71^+$ and $MHCII^+$ MDMs (Fig. 4C and 4D), and restored stroke-induced changes in the population of $CD71^+$ and $MHCII^+$ TRMs in the gut of both young

and aged stroked mice (Fig. 4C and 4D). We also assessed $CD71^+$, $MHCII^+$ P1, P2 and P3 macrophages, and while we did not detect $CD71^+$, $MHCII^+$ P1 and P3 macrophages in both young and aged mice, NR increased the populations of $CD71^+$ and $MHCII^+$ P2 macrophages in young stroked mice and restored these populations in aged stroked mice (Fig. 4E and 4F).

Finally, we evaluated overall intestinal inflammation and determined that NR had no effect on general inflammation in the gut of young mice 24 hours after stroke (Figure S6D). However, in the gut of aged stroked mice, NR restored the expression of several immune factors to sham levels 24 hours after stroke, thus reducing inflammation in the gut (Figure S6E). Together, these results suggest that NR administration prior to stroke protects against stroke-induced decline in intestinal macrophages and reduces gut inflammation.

Nicotinamide riboside reduces stroke-induced gut permeability in aged mice.

Stroke compromises gut barrier integrity by triggering adrenergic signals to the intestine, causing a transient but consequential disruption of the gut epithelium. This allows the translocation of microbial components across the gut epithelium and hyperactivation of lamina propria macrophages, and this persistent gut barrier damage increases the risk of bacterial infection and worsens stroke outcomes.[14, 15, 33] Given the effect of NR on monocyte/macrophage cell populations in the gut, we next tested whether gut permeability might be improved following NR pretreatment. Fluorescein isothiocyanate-labeled dextran (FITC-Dextran) was orally administered to sham, vehicle and NR-treated young and aged stroked at 24 hours post stroke, and levels measured in the blood plasma 4 hours later. NR treatment did not alter plasma FITC-Dextran levels in young stroked mice. However, in aged stroked mice, NR administration resulted in FITC-Dextran levels comparable to sham mice, indicating reduced gut barrier permeability relative to vehicle-treated stroked mice (Fig. 5A). To confirm these beneficial effects of NR on gut barrier integrity, we measured endotoxin lipopolysaccharide (LPS) levels in plasma 24 hours after stroke. No differences were observed in young mice, however, endotoxin levels were significantly reduced in NR-treated aged compared to vehicle-treated stroked mice (Fig. 5B), confirming that NR rescued stroke-induced increases in gut barrier permeability.

To further probe the integrity of the gut epithelium, we immunostained for tight junction proteins, zona occludens-1 (ZO-1) and epithelial cell adhesion molecule (EpCAM), and probed for CD11b, a marker for resident macrophages. NR had no effect on levels of ZO-1 and EpCAM but restored expression of CD11b to sham levels in the young stroked mice (Fig. 5C and 5D). In aged stroked mice, NR restored expression of ZO-1 and CD11b to sham levels, and marginally increased EpCAM (Fig. 5C and 5D).

To assess whether improved gut integrity was linked to changes in NAD^+, we measured levels of NAD^+ and nicotinic acid (NA), which studies have shown increases as a result of NR metabolism by the gut microbiome[29] (Fig. 5E). In the gut from young mice, no differences were observed in NA or NAD^+ levels between sham, vehicle and NR-treated stroked mice, however, both NA and NAD^+ levels were significantly increased in the gut of aged NR-treated stroked mice compared to sham and vehicle-treated stroked mice (Fig. 5F). These findings support highly beneficial effects of NR pretreatment in aged stroked mice with protection of gut barrier function.

Nicotinamide riboside improves stroke induced motor deficits.

Given the improved metabolism and reduced inflammation in aged stroked mice from NR pretreatment, we then assessed other measures of stroke severity. We evaluated motor coordination and balance by subjecting sham, vehicle and NR-treated young and aged mice to a rotarod test, which measures the latency to fall from an accelerating/decelerating rotating rod, 24 hours after stroke. The latency to fall from the rotarod was improved in NR-treated young stroked mice in the first trial, however by the third trial, there were no significant differences between sham, vehicle and NR-treated young stroked mice (Fig. 6A). Likewise, NR-treated aged stroked mice performed better in the first trial compared to sham and vehicle-treated stroked mice (Fig. 6B). Next, we reversed the direction of motion of the rotarod to challenge motor coordination and determine if the mice would self-correct and remain on the rotarod. For both young and aged mice, NR-treated mice had a higher latency to fall compared to sham and vehicle-treated stroked mice (Fig. 6A and 6B).

In line with this improved motor control, we also observed that infarct area, measured at 24 hours after stroke, was reduced in NR-treated young and aged stroked mice compared with sham and vehicle-treated stroked mice (Fig. 6C and 6D). We also investigated the number of IBA1-positive cells expressing CD68 to measure activation of microglia in the infarct area. In the young, NR marginally decreased expression of IBA1 and CD68 (Fig. 6E), and in aged NR-treated stroked mice, both IBA1 and CD68 expression were significantly reduced compared to vehicle-treated stroked mice (Fig. 6F). Interestingly, the ratio of CD68/IBA1 expression was unchanged in both young and aged NR-treated stroked mice, suggesting that NR had no effect on overall microglial activation. Altogether, NR pretreatment protects against stroke-related motor deficits and reduces stroke infarct size in both young and aged mice.

DISCUSSION

The precise cause of the robust and maladaptive inflammatory response to stroke in aged individuals is unclear. This is the first study to investigate the metabolism of blood monocytes and evaluate the effect of boosting NAD^+ levels on the response of peripheral blood

monocytes to stroke. Nicotinamide riboside (NR) has been shown to enhance NAD^+ levels and alter the metabolism and inflammatory status of human blood monocytes by increasing purine levels required for nucleotide synthesis.[28] Here, we find that prolonged pretreatment with NR prior to stroke reduces detrimental age-dependent metabolic and inflammatory changes in blood monocytes and prevents post-stroke increases in gut barrier permeability. Our studies demonstrate that stroke triggers age-dependent metabolic changes in blood monocytes by reducing NAD^+ levels and increasing levels of the neurotoxic quinolinic acid (QA). NR supplementation improves stroke outcomes by broadly replenishing NAD^+ levels in blood monocytes, intestine, and brain, while mitigating inflammation and endotoxemia caused by gut barrier disruption.

Several studies have investigated acute and chronic transcriptomic and inflammatory changes of immune cells in the blood and brain-infarct areas of young and aged mice after stroke,[3, 14, 37] however, the metabolic status of immune cells after stroke has not been explored. In this study, we focused on peripheral blood monocytes because these cells infiltrate the brain in response to stroke, alongside neutrophils, to drive secondary stroke injury. Because of the link between metabolism and immune function, we investigated the metabolic state of blood monocytes immediately post-stroke during the period in which they traffic to the ischemic brain. Our results reveal age-dependent metabolic and inflammatory changes over time, with the most pronounced changes occurring 24 hours post stroke.

While several metabolites changed over time in both young and aged blood monocytes, the NAD^+ metabolome was altered across all time points only in aged stroked mice, leading us to investigate NAD^+ biosynthetic pathways, including the Kynurenine pathway (KP). Activation of the KP correlates with increased stroke severity.[22] QA is generated by the KP and the elevated levels of QA in aged blood monocytes observed in our study support both the activation of the KP in monocytes after stroke as well as the failure to convert to the NAD^+ precursor, nicotinic acid mononucleotide (NaMN). In the brain, QA induces excitotoxicity in neurons by activating NMDA receptors.[24] QA can also reduce nucleotide levels including GTP, ATP and NAD^+, leading to mitochondrial dysfunction in synapses and neuronal damage.[38] The increased monocytic QA level in aged mice could potentially worsen excitatory injury following trafficking to the ischemic brain.

Replenishing NAD^+ levels is neuroprotective in young mouse models of stroke and in aging.[39–43] We investigated the effects of NR supplementation on stroke outcome in young and aged mice, focusing on the effects on blood monocytes and gut barrier integrity. The choice of NR compared to nicotinamide (NAM) and nicotinamide mononucleotide (NMN) was made due to its robust enhancement of mitochondrial function, the feasibility of daily oral administration, avoidance of the side effects associated with NAM, and the instability of NMN.[26, 44] Prolonged daily NR pretreatment in aged mice enhanced basal respiration, ATP production, and glycolytic activity and reduced expression of multiple pro-inflammatory molecules in blood monocytes following stroke. Additionally, increased NaMN and decreased QA levels in aged blood monocytes suggested enhanced KP metabolic flux. Overall, NR had a more potent effect on aged mice compared to young mice as the elevated levels of inflammatory mediators in both blood monocytes and plasma were most reduced in aged mice.

Increased gut permeability and dysbiosis are significant contributors to neuroinflammation and worse stroke outcomes in aging.[14, 15, 33, 45] While NR did not show any measurable effects in young mice, it reduced gut permeability in aged stroked mice. Indeed, NR has been shown to improve ethanol-induced gut barrier damage via mitochondrial sirtuins in intestinal epithelial cells.[46] Moreover, in aged mice, pretreatment with NR completely prevented age-associated losses of MDMs and TRMs in the intestinal lamina propria which are critical to gut barrier function. The improvement in gut barrier function observed in aged NR-pretreated stroked mice may be the result of improved overall epithelial health from increased absorption of NR and NMN, as well as improved MDM and TRM immune states, as reflected by reversal of inflammatory markers $CD71^+$ and $MHCII^+$.

Alongside the overall improved immune state of monocytes and intestinal macrophages, NR pretreatment also improved motor coordination in both young and aged stroked mice, reduced infarct size and mitigated inflammation in the brain. A recent study performed in young mice demonstrated reduced stroke infarct volume with a single post-ischemic NR treatment, but poorer stroke outcomes with three days of pre-ischemic NR treatment.[42] In that study, it is possible that the timing was not sufficient for cells to metabolically adapt to such high levels of NAD^+ prior to the ischemic event. The authors also observed improved outcome with a single post-ischemic dose of Nam, however, it is important to note that several other studies have demonstrated Nam inhibition of sirtuins, essential mediators of metabolic homeostasis, as well as adverse effects of Nam on liver function.[44, 47]

A limitation of the current study is that only male mice were examined. There are well established mechanistic differences between male and female responses to stroke,[48] and potential sex-specific metabolic differences will be explored in future studies. Regarding the metabolism of NR, further studies are required to understand how NR is metabolized in the gut by the gut microbiome after stroke. It is known that NR is converted to nicotinamide mononucleotide (NMN) by nicotinamide riboside kinase (NRK1) and then to NAD^+, however, oral administration of NR leads to an increase in nicotinic acid (NA) which is metabolized to nicotinic acid mononucleotide (NaMN) by the gut microbiome,[26, 29, 49] a common metabolite of the Kynurenine (KP) and Preiss-Handler pathways, suggesting activation of either pathway by NR through a

mechanism that is not fully understood. Another limitation is the technical challenge in measuring NAD^+ levels in very small samples such as blood monocytes due to its rapid turnover, low analyte concentration and instability. To address this limitation, we measured NaMN as a readout for increased NAD^+ levels when undetected, given that orally administered NR has been shown to significantly increase NaMN.[26, 29]

In conclusion, we identified age-related metabolic alterations in monocytes following stroke, characterized by reduced NAD^+ and elevated QA levels, which were associated with changes in inflammatory factors. Additionally, we showed that prolonged NR pretreatment effectively replenishes NAD^+, enhances the metabolic and inflammatory responses of blood monocytes to stroke, and broadly improves stroke outcomes by strengthening gut barrier function and reducing inflammation. Our findings highlight the potential of NR as a preventive therapeutic strategy for patients at high risk of cardiovascular and cerebrovascular disease.

Declarations

Competing Interests

The authors declare that they have no competing interests.

Authors and Affiliations

Department of Pharmacology, Case Western Reserve University School of Medicine, Cleveland, OH, USA (C.A.I., B.A.E), Department of Neurology and Neurological Science, Stanford University School of Medicine, Stanford, CA, USA (C.A.I., K.I.A., M.C., J.H., H.E.E., Y.A.A., Q.W.), Wu Tsai Neurosciences Institute, Stanford University, Stanford, CA, USA (K.I.A.), Stanford Neurosciences Graduate Program, Stanford University, Stanford, CA, USA (J.H.), Mass Spectrometry Center, Stanford University, Stanford, CA, USA (L.A.), Department of Biochemistry and Molecular Biology, Huck Institutes of the Life Sciences, Pennsylvania State University, University Park, PA, USA (A.I.A., M.R.M.), Department of Molecular Biosciences, The University of Texas at Austin, TX, USA (M.C.), Department of Biological Chemistry, The Hebrew University of Jerusalem, Jerusalem, Israel (E.B.), Chan Zuckerberg Biohub, San Francisco, CA, USA (K.A.I).

Funding sources

This work was supported by Burroughs Wellcome Postdoctoral Diversity Enrichment Program grant no. G-1022372 (C.A.I). The Howard Hughes Medical Institute Hanna H. Gray Fellows Program Faculty Phase grant no. GT15655 (M.R.M). The Burroughs Welcome Fund PDEP Transition to Faculty grant no. 1022604 (M.R.M). NIH Grants T32GM108563 (A.I.A.), RO1NS100180 (K.I.A.). The American Heart Foundation grant no. 19PABH1345800 (K.I.A.). K.I.A. is a Chan Zuckerberg–San Francisco Biohub Investigator.

Author Contribution

C.A.I and K.I.A. conceived and planned this study. C.A.I., M.R.M., and K.I.A. contributed to supervising the experimental design. C.A.I., H.E., M.C., A.I.A., L.A., Y.A.A., Q.W., and E.B. conducted the experiments. C.A.I., H.E., M.C., A.I.A., L.A., J.H., B.A.E, and M.R.M performed collection of the data and statistical analysis. C.A.I. and K.I.A. wrote the manuscript. All authors reviewed and approved of the manuscript.

Acknowledgments

We would like to acknowledge the Stanford University Mass Spectrometry core facility for the use of the Xevo TQ-XS mass spectrometer system (RRID:SCR_018510) that was purchased with funding from National Institutes of Health Shared Instrumentation Grant S10OD026962. We thank the Stanford University Cell Sciences Imaging Core Facility for the use of the Leica SP8 confocal microscope (RRID: SCR_017787), supported by the Award Number 1S10OD010580-01A1 from the National Center for Research Resources (NCRR). We would also like to acknowledge the Stanford University Human Immune Monitoring Center (HIMC) and the Case Western Reserve University Bioanalyte core facility for the Luminex experiments. We would also like to acknowledge the Huck Institutes' Metabolomics core facility (RRID:SCR_023864) for use of the OE 240 LC-MS and Sergei Koshkin for helpful discussions on sample preparation and analysis. Finally, we thank Chromadex for providing the Nicotinamide Riboside used in this study.

Availability of data and materials

The datasets used and analyzed during the current study are included in this published article and are available from the corresponding author on reasonable request.

References

1. Offner H, Subramanian S, Parker SM, Afentoulis ME, Vandenbark AA, Hurn PD. Experimental stroke induces massive, rapid activation of the peripheral immune system. J Cereb Blood Flow Metab. 2006;26(5):654–65. PubMed PMID: 16121126. Epub 2005/08/27.
2. Ritzel RM, Lai YJ, Crapser JD, Patel AR, Schrecengost A, Grenier JM, et al. Aging alters the immunological response to ischemic stroke. Acta Neuropathol. 2018;136(1):89–110. PubMed PMID: 29752550. PMCID: PMC6015099. Epub 20180511.
3. Androvic P, Kirdajova D, Tureckova J, Zucha D, Rohlova E, Abaffy P, et al. Decoding the Transcriptional Response to Ischemic Stroke in Young and Aged Mouse Brain. Cell Rep. 2020;31(11):107777. PubMed PMID: 32553170.
4. O'Neill LA, Kishton RJ, Rathmell J. A guide to immunometabolism for immunologists. Nat Rev Immunol. 2016;16(9):553–65. PubMed PMID: 27396447. PMCID: PMC5001910. Epub 20160711.
5. Minhas PS, Liu L, Moon PK, Joshi AU, Dove C, Mhatre S, et al. Macrophage de novo NAD(+) synthesis specifies immune function in aging and inflammation. Nat Immunol. 2019;20(1):50–63. PubMed PMID: 30478397. PMCID: PMC6768398. Epub 2018/11/28.
6. Jha AK, Huang SC, Sergushichev A, Lampropoulou V, Ivanova Y, Loginicheva E, et al. Network integration of parallel metabolic and transcriptional data reveals metabolic modules that regulate macrophage polarization. Immunity. 2015;42(3):419–30. PubMed PMID: 25786174.
7. Wculek SK, Heras-Murillo I, Mastrangelo A, Mananes D, Galan M, Miguel V, et al. Oxidative phosphorylation selectively orchestrates tissue macrophage homeostasis. Immunity. 2023;56(3):516–30. e9. PubMed PMID: 36738738. Epub 20230203.
8. Palsson-McDermott EM, Curtis AM, Goel G, Lauterbach MA, Sheedy FJ, Gleeson LE, et al. Pyruvate kinase M2 regulates Hif-1alpha activity and IL-1beta induction and is a critical determinant of the warburg effect in LPS-activated macrophages. Cell Metab. 2015;21(1):65–80. PubMed PMID: 25565206. PMCID: PMC5198835.
9. Cheng SC, Quintin J, Cramer RA, Shepardson KM, Saeed S, Kumar V, et al. mTOR- and HIF-1alpha-mediated aerobic glycolysis as metabolic basis for trained immunity. Science. 2014;345(6204):1250684. PubMed PMID: 25258083. PMCID: PMC4226238.
10. Canto C, Houtkooper RH, Pirinen E, Youn DY, Oosterveer MH, Cen Y, et al. The NAD(+) precursor nicotinamide riboside enhances oxidative metabolism and protects against high-fat diet-induced obesity. Cell Metab. 2012;15(6):838–47. PubMed PMID: 22682224. PMCID: PMC3616313. Epub 2012/06/12.
11. Roboon J, Hattori T, Ishii H, Takarada-Iemata M, Nguyen DT, Heer CD, et al. Inhibition of CD38 and supplementation of nicotinamide riboside ameliorate lipopolysaccharide-induced microglial and astrocytic neuroinflammation by increasing NAD(). J Neurochem. 2021;158(2):311–27. PubMed PMID: 33871064. PMCID: PMC8282715. Epub 20210509.
12. Bain CC, Schridde A. Origin, Differentiation, and Function of Intestinal Macrophages. Front Immunol. 2018;9:2733. PubMed PMID: 30538701. PMCID: PMC6277706. Epub 20181127.
13. Bujko A, Atlasy N, Landsverk OJB, Richter L, Yaqub S, Horneland R, et al. Transcriptional and functional profiling defines human small intestinal macrophage subsets. J Exp Med. 2018;215(2):441–58. PubMed PMID: 29273642. PMCID: PMC5789404. Epub 20171222.
14. Liu Q, Johnson EM, Lam RK, Wang Q, Bo Ye H, Wilson EN, et al. Peripheral TREM1 responses to brain and intestinal immunogens amplify stroke severity. Nat Immunol. 2019;20(8):1023–34. PubMed PMID: 31263278. PMCID: PMC6778967. Epub 2019/07/03.
15. Crapser J, Ritzel R, Verma R, Venna VR, Liu F, Chauhan A, et al. Ischemic stroke induces gut permeability and enhances bacterial translocation leading to sepsis in aged mice. Aging. 2016;8(5):1049–63. PubMed PMID: 27115295. PMCID: PMC4931853.
16. Llovera G, Roth S, Plesnila N, Veltkamp R, Liesz A. Modeling stroke in mice: permanent coagulation of the distal middle cerebral artery. J Vis Exp 2014 Jul 31(89):e51729. PubMed PMID: 25145316. PMCID: PMC4692348. Epub 2014/08/26.
17. Wang L, Xing X, Chen L, Yang L, Su X, Rabitz H, et al. Peak Annotation and Verification Engine for Untargeted LC-MS Metabolomics. Anal Chem. 2019;91(3):1838–46. PubMed PMID: 30586294. PMCID: PMC6501219. Epub 2018/12/27.
18. Adusumilli R, Mallick P. Data Conversion with ProteoWizard msConvert. Methods Mol Biol. 2017;1550:339 – 68. PubMed PMID: 28188540. Epub 2017/02/12.
19. Liang X, Yang L, Qin AR, Ly J, Liederer BM, Messick K, et al. Measuring NAD(+) levels in mouse blood and tissue samples via a surrogate matrix approach using LC-MS/MS. Bioanalysis. 2014;6(11):1445–57. PubMed PMID: 25046046.
20. Grahnert A, Grahnert A, Klein C, Schilling E, Wehrhahn J, Hauschildt S, Review. NAD +: a modulator of immune functions. Innate Immun. 2011;17(2):212–33. PubMed PMID: 20388721. Epub 2010/04/15.
21. Verdin E. NAD(+) in aging, metabolism, and neurodegeneration. Science. 2015;350(6265):1208–13. PubMed PMID: 26785480. Epub 2016/01/20.

22. Darlington LG, Mackay GM, Forrest CM, Stoy N, George C, Stone TW. Altered kynurenine metabolism correlates with infarct volume in stroke. Eur J Neurosci. 2007;26(8):2211–21. PubMed PMID: 17892481. Epub 2007/09/26.
23. Brouns R, Verkerk R, Aerts T, De Surgeloose D, Wauters A, Scharpe S, et al. The role of tryptophan catabolism along the kynurenine pathway in acute ischemic stroke. Neurochem Res. 2010;35(9):1315–22. PubMed PMID: 20490917. Epub 2010/05/22.
24. Guillemin GJ. Quinolinic acid, the inescapable neurotoxin. FEBS J. 2012;279(8):1356–65. PubMed PMID: 22248144. Epub 2012/01/18.
25. Guillemin GJ, Croitoru-Lamoury J, Dormont D, Armati PJ, Brew BJ. Quinolinic acid upregulates chemokine production and chemokine receptor expression in astrocytes. Glia. 2003;41(4):371–81. PubMed PMID: 12555204.
26. Trammell SA, Schmidt MS, Weidemann BJ, Redpath P, Jaksch F, Dellinger RW et al. Nicotinamide riboside is uniquely and orally bioavailable in mice and humans. Nat Commun 2016;7:12948. PubMed PMID: 27721479. PMCID: PMC5062546 Epub 2016/10/11.
27. Cheng YH, Zhao JH, Zong WF, Wei XJ, Xu Z, Yuan Y, et al. Acute Treatment with Nicotinamide Riboside Chloride Reduces Hippocampal Damage and Preserves the Cognitive Function of Mice with Ischemic Injury. Neurochem Res. 2022;47(8):2244–53. PubMed PMID: 35585298. Epub 20220519.
28. Wu J, Singh K, Lin A, Meadows AM, Wu K, Shing V et al. Boosting NAD + blunts TLR4-induced type I IFN in control and systemic lupus erythematosus monocytes. J Clin Invest. 2022;132(5). PubMed PMID: 35025762. PMCID: PMC8884917.
29. Shats I, Williams JG, Liu J, Makarov MV, Wu X, Lih FB, et al. Bacteria Boost Mammalian Host NAD Metabolism by Engaging the Deamidated Biosynthesis Pathway. Cell Metab. 2020;31(3):564–79. e7. PubMed PMID: 32130883. PMCID: PMC7194078.
30. Jia T, Serbina NV, Brandl K, Zhong MX, Leiner IM, Charo IF, et al. Additive roles for MCP-1 and MCP-3 in CCR2-mediated recruitment of inflammatory monocytes during Listeria monocytogenes infection. J Immunol. 2008;180(10):6846–53. PubMed PMID: 18453605. PMCID: PMC2386263. Epub 2008/05/06.
31. Boulakirba S, Pfeifer A, Mhaidly R, Obba S, Goulard M, Schmitt T, et al. IL-34 and CSF-1 display an equivalent macrophage differentiation ability but a different polarization potential. Sci Rep. 2018;8(1):256. PubMed PMID: 29321503. PMCID: PMC5762882. Epub 20180110.
32. Adankwah E, Harelimana JD, Minadzi D, Aniagyei W, Abass MK, Batsa Debrah L, et al. Lower IL-7 Receptor Expression of Monocytes Impairs Antimycobacterial Effector Functions in Patients with Tuberculosis. J Immunol. 2021;206(10):2430–40. PubMed PMID: 33911006. Epub 20210428.
33. Wang H, Li J, Wu G, Lin X, Chen J, Liang J, et al. Activated sympathetic nerve post stroke downregulates Toll-like receptor 5 and disrupts the gut mucosal barrier. Cell Rep Med. 2024;5(10):101754. PubMed PMID: 39383869. PMCID: PMC11513850. Epub 20241008.
34. Schridde A, Bain CC, Mayer JU, Montgomery J, Pollet E, Denecke B, et al. Tissue-specific differentiation of colonic macrophages requires TGFbeta receptor-mediated signaling. Mucosal Immunol. 2017;10(6):1387–99. PubMed PMID: 28145440. PMCID: PMC5417360. Epub 20170201.
35. Allden SJ, Ogger PP, Ghai P, McErlean P, Hewitt R, Toshner R, et al. The Transferrin Receptor CD71 Delineates Functionally Distinct Airway Macrophage Subsets during Idiopathic Pulmonary Fibrosis. Am J Respir Crit Care Med. 2019;200(2):209–19. PubMed PMID: 31051082. PMCID: PMC6635794.
36. Guillaume J, Leufgen A, Hager FT, Pabst O, Cerovic V. MHCII expression on gut macrophages supports T cell homeostasis and is regulated by microbiota and ontogeny. Sci Rep. 2023;13(1):1509. PubMed PMID: 36707699. PMCID: PMC9883227. Epub 20230127.
37. Garcia-Bonilla L, Shahanoor Z, Sciortino R, Nazarzoda O, Racchumi G, Iadecola C, et al. Analysis of brain and blood single-cell transcriptomics in acute and subacute phases after experimental stroke. Nat Immunol. 2024;25(2):357–70. PubMed PMID: 38177281. Epub 20240104.
38. Bordelon YM, Chesselet MF, Nelson D, Welsh F, Erecinska M. Energetic dysfunction in quinolinic acid-lesioned rat striatum. J Neurochem. 1997;69(4):1629–39. PubMed PMID: 9326292.
39. Zhao Y, Guan YF, Zhou XM, Li GQ, Li ZY, Zhou CC, et al. Regenerative Neurogenesis After Ischemic Stroke Promoted by Nicotinamide Phosphoribosyltransferase-Nicotinamide Adenine Dinucleotide Cascade. Stroke. 2015;46(7):1966–74. PubMed PMID: 26060246. Epub 20150609.
40. Park JH, Long A, Owens K, Kristian T. Nicotinamide mononucleotide inhibits post-ischemic NAD(+) degradation and dramatically ameliorates brain damage following global cerebral ischemia. Neurobiol Dis. 2016;95:102 – 10. PubMed PMID: 27425894. PMCID: PMC5580241. Epub 20160715.
41. Wang C, Zhang Y, Ding J, Zhao Z, Qian C, Luan Y et al. Nicotinamide Administration Improves Remyelination after Stroke. Neural Plast. 2017;2017:7019803. PubMed PMID: 28656112. PMCID: PMC5471593. Epub 20170601.
42. Qu W, Ralto KM, Qin T, Cheng Y, Zong W, Luo X, et al. NAD(+) precursor nutritional supplements sensitize the brain to future ischemic events. J Cereb Blood Flow Metab. 2023;43(2suppl):37–48. PubMed PMID: 37434361. PMCID: PMC10638999. Epub 20230222.
43. Martens CR, Denman BA, Mazzo MR, Armstrong ML, Reisdorph N, McQueen MB, et al. Chronic nicotinamide riboside supplementation is well-tolerated and elevates NAD(+) in healthy middle-aged and older adults. Nat Commun. 2018;9(1):1286. PubMed PMID: 29599478.

PMCID: PMC5876407. Epub 20180329.

44. Kang-Lee YA, McKee RW, Wright SM, Swendseid ME, Jenden DJ, Jope RS. Metabolic effects of nicotinamide administration in rats. J Nutr. 1983;113(2):215–21. PubMed PMID: 6218261.
45. Singh V, Roth S, Llovera G, Sadler R, Garzetti D, Stecher B, et al. Microbiota Dysbiosis Controls the Neuroinflammatory Response after Stroke. J Neurosci. 2016;36(28):7428–40. PubMed PMID: 27413153. PMCID: PMC6705544.
46. Li W, Zhou Y, Pang N, Hu Q, Li Q, Sun Y et al. NAD Supplement Alleviates Intestinal Barrier Injury Induced by Ethanol Via Protecting Epithelial Mitochondrial Function. Nutrients. 2022;15(1). PubMed PMID: 36615829. PMCID: PMC9823589. Epub 20221230.
47. Chang HC, Guarente L. SIRT1 and other sirtuins in metabolism. Trends Endocrinol Metab. 2014;25(3):138–45. PubMed PMID: 24388149. PMCID: PMC3943707. Epub 20131230.
48. Rexrode KM, Madsen TE, Yu AYX, Carcel C, Lichtman JH, Miller EC. The Impact of Sex and Gender on Stroke. Circ Res. 2022;130(4):512–28. PubMed PMID: 35175851. PMCID: PMC8890686. Epub 20220217.
49. Peluso AA, Lundgaard AT, Babaei P, Mousovich-Neto F, Rocha AL, Damgaard MV, et al. Oral supplementation of nicotinamide riboside alters intestinal microbial composition in rats and mice, but not humans. NPJ Aging. 2023;9(1):7. PubMed PMID: 37012386. PMCID: PMC10070358. Epub 20230403.

Figures

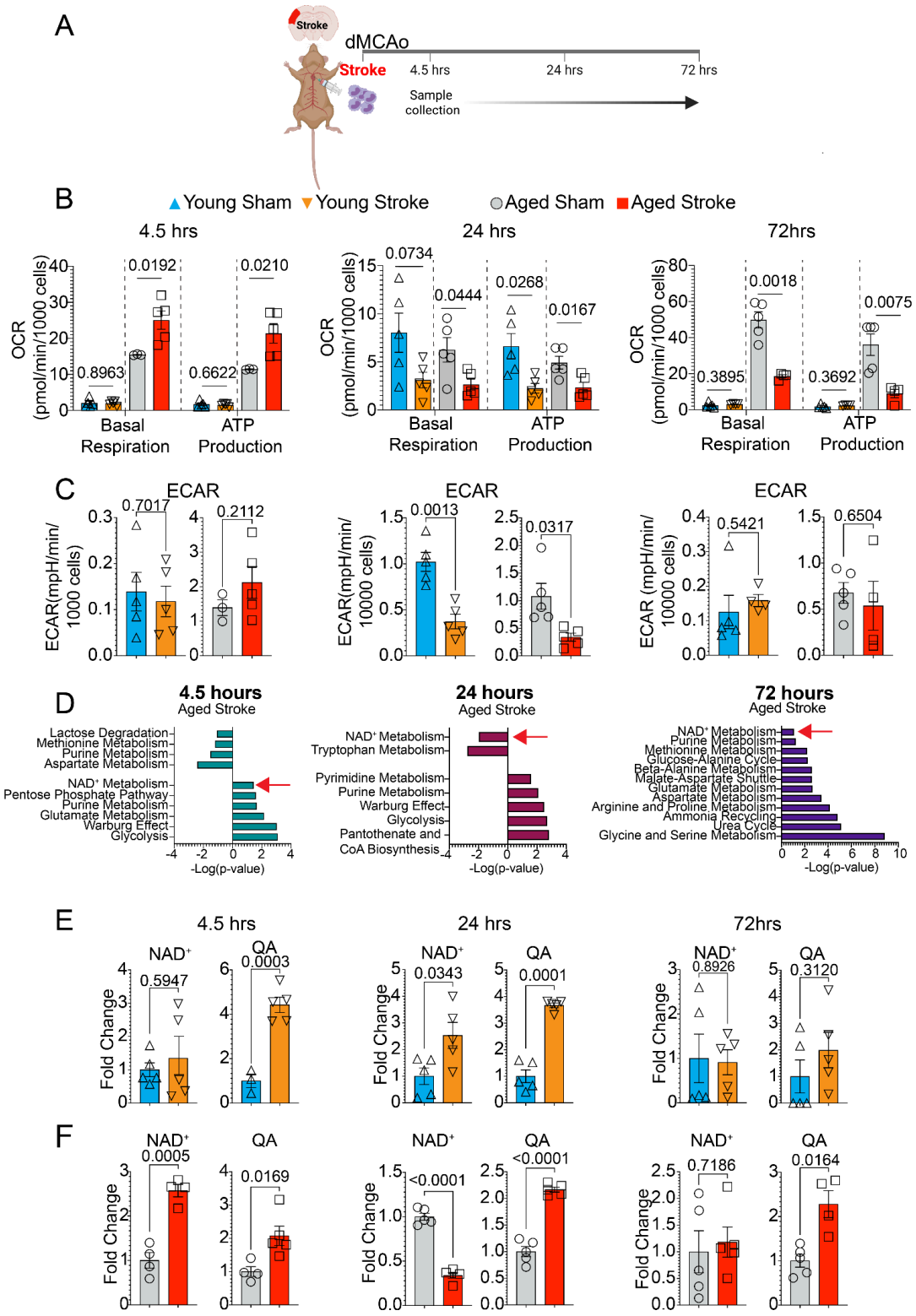


Figure 1

Time course of bioenergetic responses of blood monocytes from young and aged mice after stroke. (A) Schematic illustrating the timeline of stroke induction using the dMCAo (distal middle cerebral artery occlusion) model, and collection of blood monocytes from young (3–6 mo) and aged (18–20 mo) mice. **(B)** Seahorse (Mitostress test) analysis of basal respiration, ATP production and **(C)** extracellular acidification rates (ECAR) of blood monocytes isolated from young and aged mice at 4.5 hours, 24 hours, and 72 hours after stroke. n=3–5 male mice per group. Data are represented as the mean ± SEM. p-values were calculated using two-tailed Student's t-test. **(D)** Analysis of enriched metabolic pathways in blood monocytes isolated from aged mice at 4.5, 24 and 72 hours after stroke. Data were analyzed using MetaboAnalyst 6.0. Red arrows indicate changes in nicotinamide adenine dinucleotide (NAD+) metabolic pathways. Negative and positive values indicate decreased and increased pathways respectively. LC-MS/MS measurement of NAD+ and quinolinic acid (QA) levels in blood monocytes isolated from **(E)**

young and **(F)** aged male mice at 4.5 hours, 24 hours and 72 hours post stroke. n=4–5 male mice per group. Data are represented as the mean ± SEM. p-values were calculated using two-tailed Student's t-test.

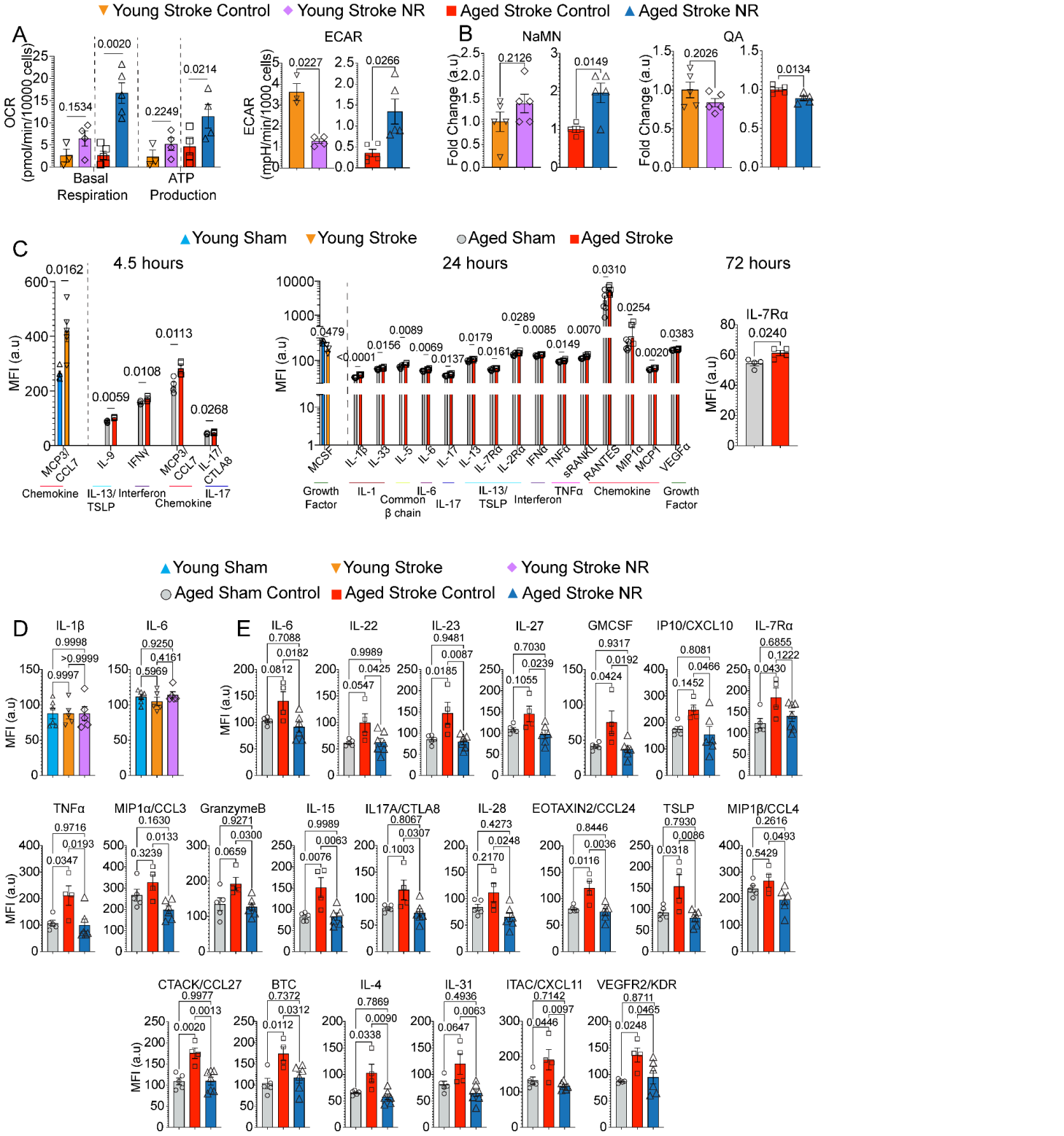
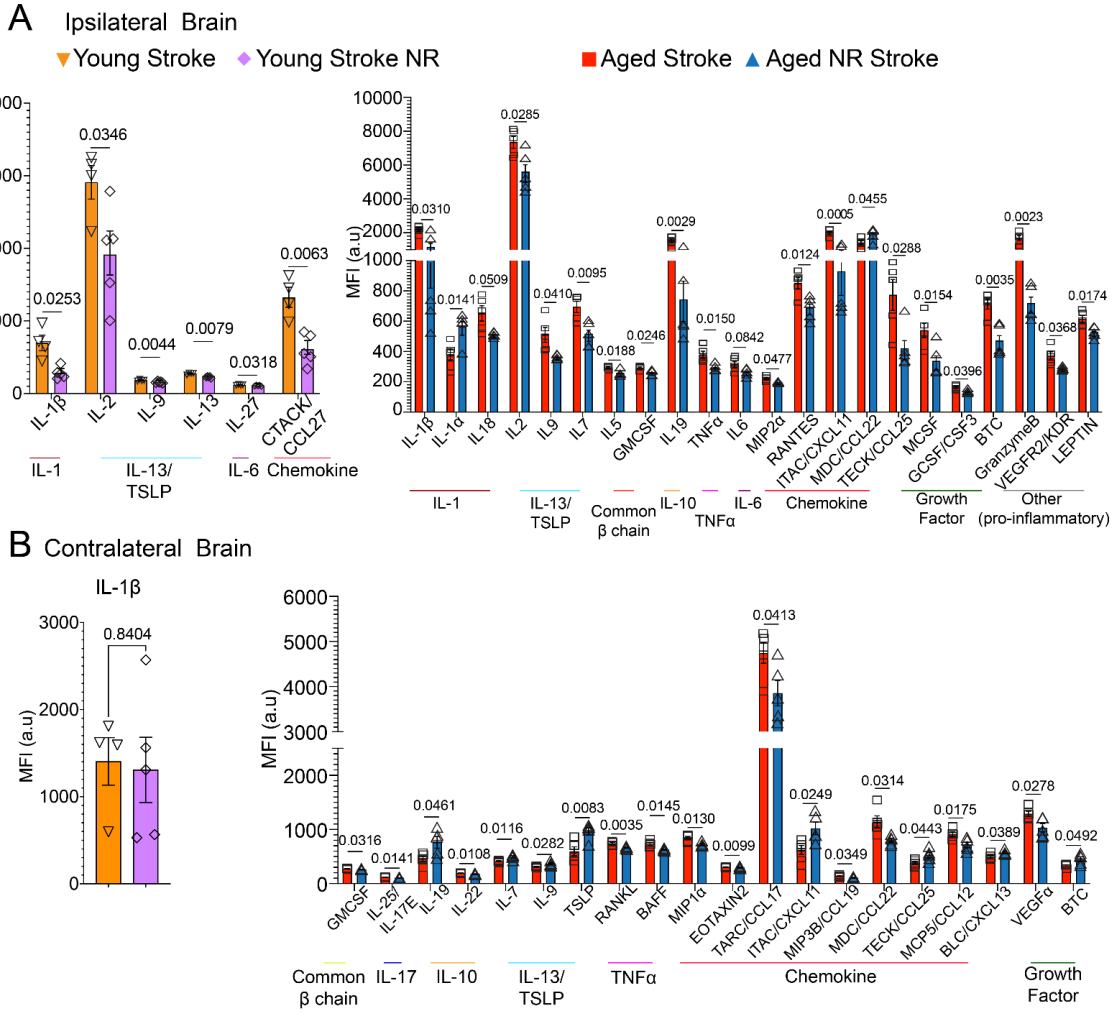


Figure 2

NAD⁺ replenishment improves metabolism of blood monocytes and reduces inflammation in aged mice after stroke. (A) Seahorse (Mitostress test) analysis of basal respiration, ATP production and extracellular acidification rates (ECAR) from blood monocytes isolated 24 hours after stroke from young (3–6 mo) and aged (18–20 mo) mice treated with either vehicle (water; control) or nicotinamide riboside (NR) via oral gavage every day for 4 weeks. n=3–5 male mice per group. Data are represented as the mean ± SEM. *p*-values were calculated using two-tailed Student's *t*-test. **(B)** LC-MS/MS measurement levels of nicotinic acid mononucleotide (NaMN; left) and quinolinic acid (QA; right) in blood monocytes isolated from control and NR-treated young and aged mice at 24 hours after stroke. n=4–5 male mice per group. Data are

represented as the mean ± SEM. *p*-values were calculated using two-tailed Student's *t*-test. **(C)** Multi-analyte cytokine/chemokine (Luminex) quantification of differences in the expression of immune factors in blood monocytes from young and aged sham and stroke mice at 4.5 hours (left), 24 hours (middle) and 72 hours (right) after stroke. n=4–5 male mice per group. Data are represented as the mean ± SEM. *p*-values were calculated using two-tailed Student's *t*-test. Multi-analyte Luminex quantification of differences in the expression of immune factors in blood monocytes isolated from sham control (vehicle; water), stroke control (vehicle; water) and stroke NR-treated **(D)** young and **(E)** aged mice 24 hours after stroke. n=4–6 male mice per group. Data are represented as the mean ± SEM. *p*-values were calculated using one-way ANOVA with Bonferroni correction.



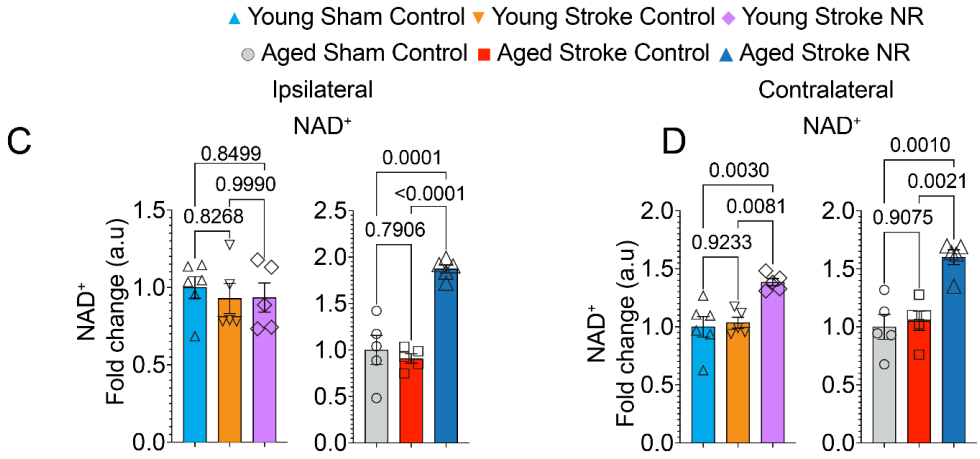


Figure 3

Nicotinamide riboside alters inflammation and increases NAD$^+$ levels in the brain after stroke. Multi-analyte Luminex quantification of differences in the expression of immune factors in the **(A)** ipsilateral and **(B)** contralateral brain isolated from vehicle (water; control) and NR-treated young (3–6 mo) and aged (18–20 mo) mice at 24 hours after stroke. n=4–5 male mice per group. Data are represented as the mean ± SEM. p-values were calculated using two-tailed Student's t-test. LC-MS/MS measurement of NAD+ levels in **(C)** ipsilateral and **(D)** contralateral brain from sham, vehicle and NR-treated young and aged mice at 24 hours post stroke. n=5 male mice per group. Data are represented as the mean ± SEM. Values were calculated using one-way ANOVA with Bonferroni correction.

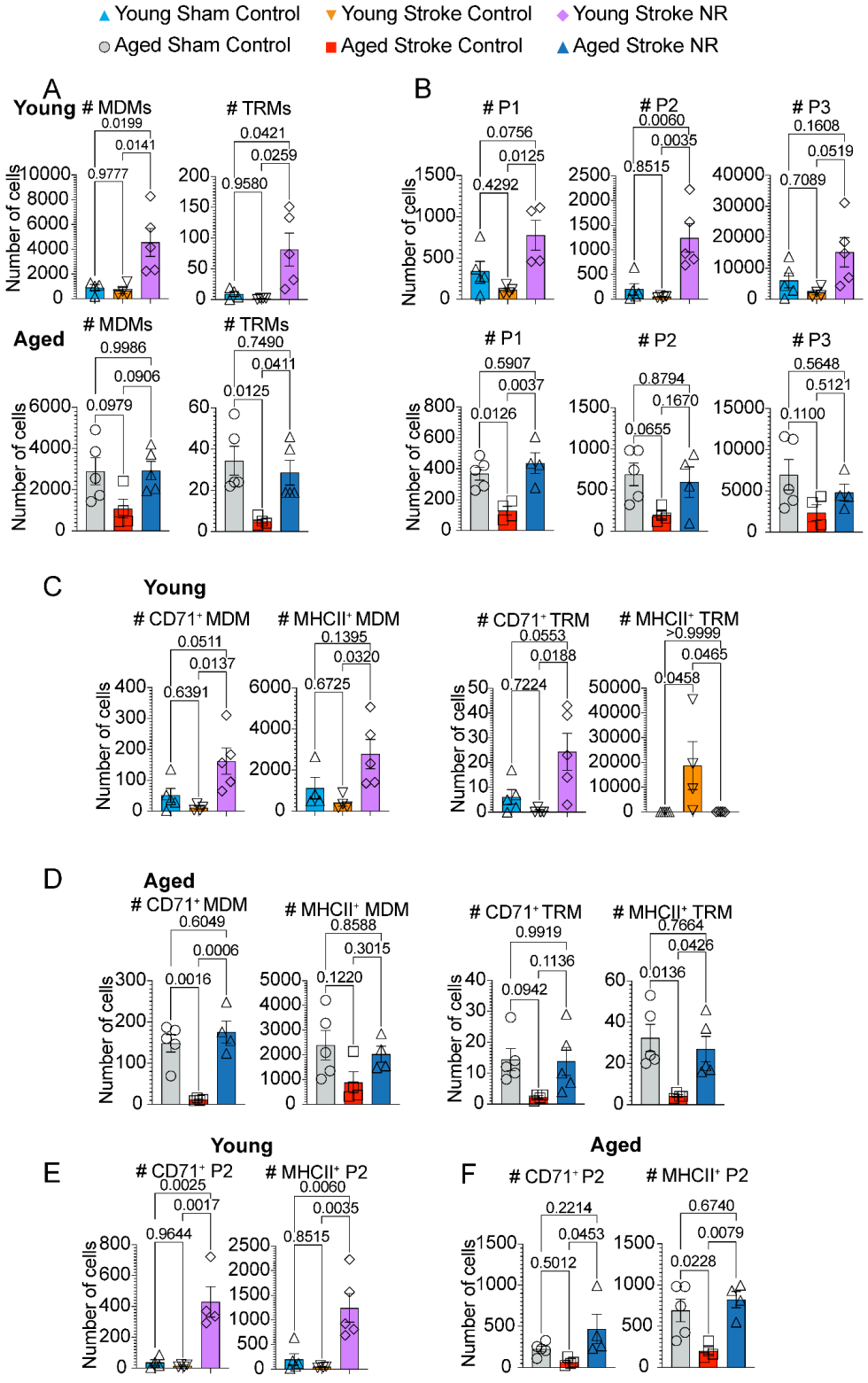


Figure 4

Nicotinamide riboside alters the composition of gut macrophages in aged mice. (A) Number of CD45^{+} monocyte-derived macrophages (MDMs) and tissue resident macrophages (TRMs) isolated from the gut of sham (vehicle; water), stroke control (vehicle; water) and stroke NR-treated young (3–6 mo; top) mice and aged (18–20 mo; bottom) mice at 24 hours after stroke. **(B)** Number of P1 (Ly6C^{Hi} MHCII^{Low}), P2 (Ly6C^{Int} MHCII^{Hi}) and P3 (Ly6C^{low} MHCII^{Hi}) macrophages in the gut of sham control, stroke control and stroke NR-treated young and aged mice. **(C)** Number of CD71^{+}, MHCII^{+} MDMs and TRMs in the gut of sham control, stroke control and stroke NR-treated young mice. **(D)** Number of CD71^{+}, MHCII^{+} MDMs and TRMs in the gut of sham control, stroke control and stroke NR-treated aged mice. **(E)** Number of CD71^{+}, MHCII^{+} P2 macrophages in the gut of sham control, stroke control and stroke NR-treated young mice. **(F)** Number of CD71^{+}, MHCII^{+} P2 macrophages in the gut of sham control, stroke control and stroke NR-treated aged mice. n=4–5 male mice per group. Data are represented as the mean ± SEM. *p*-values were calculated using one-way ANOVA with Bonferroni correction.

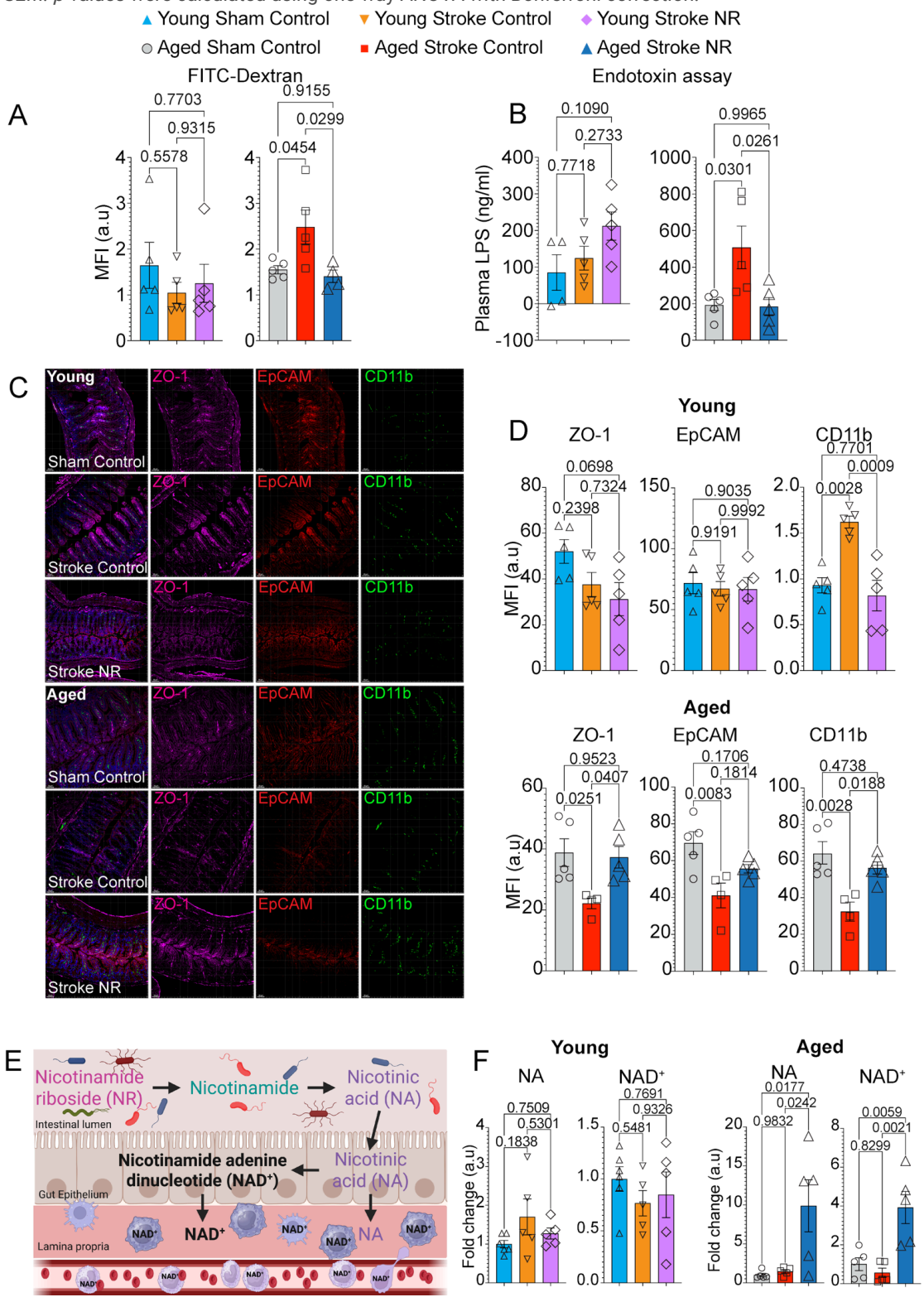


Figure 5

Nicotinamide riboside restores gut integrity in aged stroke mice. (A) FITC-Dextran was measured in the blood plasma from sham control (vehicle; water), stroke control (vehicle; water), and stroke NR-treated young (3–6 mo) and aged (18–20 mo) mice 24 hours after stroke. n=4–5 male mice per group. Data are represented as the mean ± SEM. *p*-values were calculated using one-way ANOVA with Bonferroni correction. **(B)** Blood plasma concentration levels of the bacterial endotoxin lipopolysaccharide (LPS) measured 24 hours after stroke in sham control, stroke control and stroke NR-treated young and aged stroke mice. n=4–5 male mice per group. Data are represented as the mean ± SEM. *p*-values were calculated using one-way ANOVA with Bonferroni correction. **(C)** Representative confocal images of ZO-1, EpCAM and CD11b in the lamina propria in sham control, stroke control and stroke NR-treated young (top) and aged (bottom) male mice 24 hours post stroke. Scale bar, 50 μm. **(D)** Mean fluorescent intensity quantification of ZO-1, EpCAM and CD11b expression 24 hours after stroke in sham control, stroke control and stroke NR-treated young (top) and aged (bottom) mice. n=4–5 male mice per group. Data are represented as the mean ± SEM. *p*-values were calculated using one-way ANOVA with Bonferroni correction. **(E)** Schematic illustrating metabolism of NR in the gut to NAD^+ (left; created in Biorender). **(F)** LC-MS/MS measurement of nicotinic acid (NA) and NAD^+ levels in sham control, stroke control and stroke NR-treated young (left) and aged (right) mice. n=5–6 male mice per group. Data are represented as the mean ± SEM. *p*-values were calculated using one-way ANOVA with Bonferroni correction.

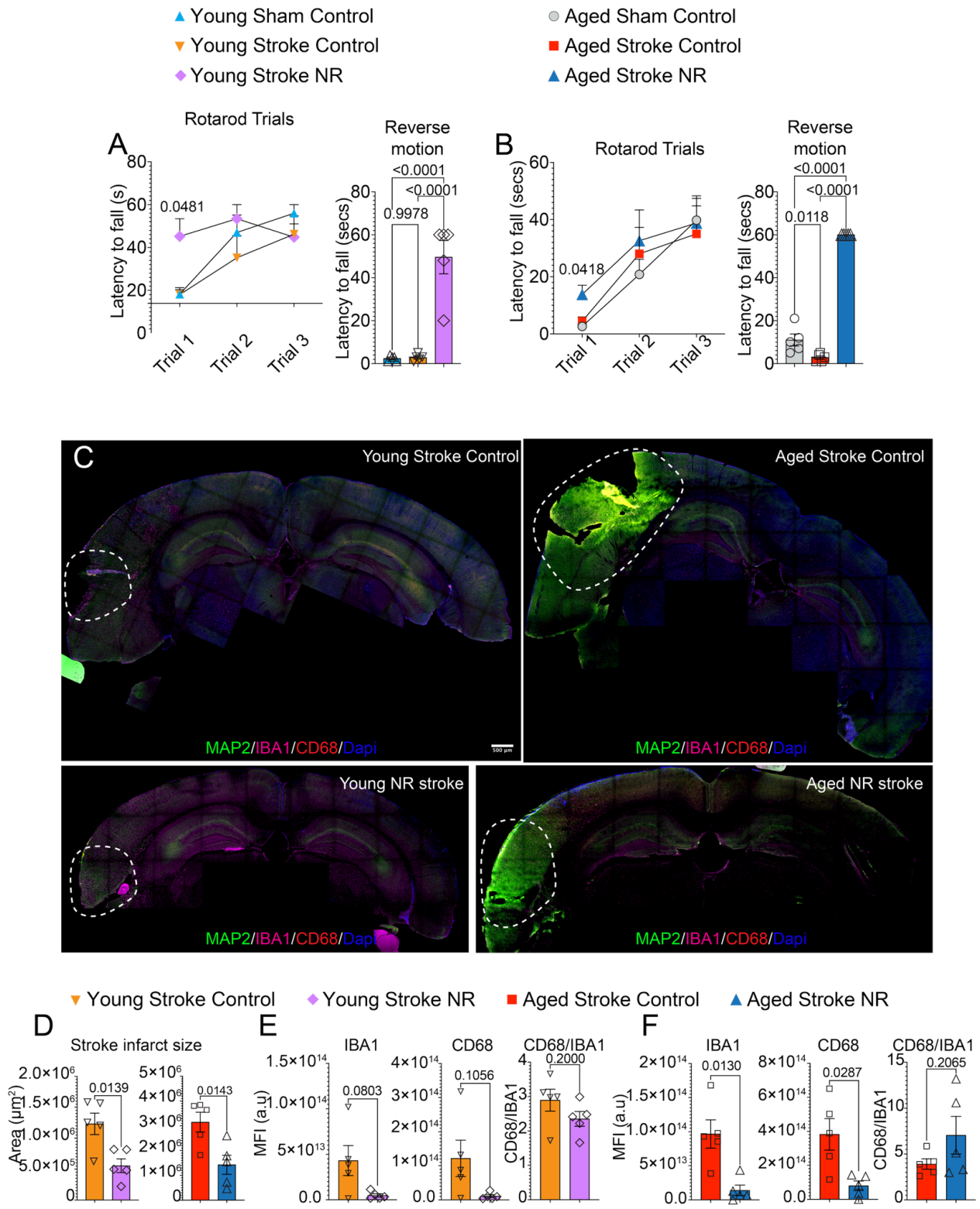


Figure 6

Nicotinamide riboside improves motor coordination and reduces stroke infarct size. Motor coordination using the rotarod test shows latency to fall in 3 trials (left graph) before stroke in sham control (vehicle; water), stroke control (vehicle; water), and stroke NR-treated **(A)** young (3–6 mo) and **(B)** aged (18–20 mo) mice 24 hours after stroke. Direction of rotarod was reversed to challenge motor coordination 24 hours after stroke (right graph). n=5 male mice per group. Data are represented as the mean ± SEM. *p*-values were calculated using one-way ANOVA with Bonferroni correction. **(C)** Representative confocal images of the brain isolated from stroke control and stroke NR-treated young and aged mice 24 hours after stroke. Brain slices were immunostained for DAPI (blue), MAP2 (neuronal marker in green), IBA1 (microglial marker, magenta) and CD68 (microglial lysosomal marker, red). **(D)** Stroke infarct size was measured as a percentage of corrected infarct area (see Methods) in young and aged stroke control and NR-treated mice at 24 hours post stroke. n=5 male mice per group. Data are represented as

the mean ± SEM. *p*-values were calculated using two-tailed Student's *t*-test. Dotted lines indicate stroke infarct area. Scale bar, 500 µm. Dotted lines show infarct area. Mean fluorescent intensity quantification of the expression and ratio of CD68 and IBA1 expression 24 hours after stroke in NR-treated **(E)** young and **(F)**aged male mice. n=5 male mice per group. Data are represented as the mean ± SEM. *p*-values were calculated using two-tailed Student's *t*-test.

Supplementary Files

This is a list of supplementary files associated with this preprint. Click to download.

- NADdepletiondrivesagerelatedmonocytehyperinflammationafterstrokeandisreversedbynicotinamideribosidesupplementarymaterials.docx